

1 **Dynamic liquefaction of shear zones in intact loess during simulated earthquake**
2 **loading**

3
4
5 **J. M. Carey¹, M. J. McSaveney¹ & D.N.Petley²**

6 ¹ *GNS Science, 1 Fairway Drive Avalon, PO Box 30368 Lower Hutt, New Zealand*

7 ² *School of Environmental Sciences, University of East Anglia, Norwich, NR4 7TJ,*
8 *UK*

9
10
11 **ABSTRACT**

12 The 2010-2011 Canterbury earthquake sequence in New Zealand exposed loess-
13 mantled slopes in the area to very high levels of seismic excitation (locally measured
14 as >2 g). Few loess slopes showed permanent local downslope deformation, and most
15 of these showed only limited accumulated displacement. A series of innovative
16 dynamic back pressured shear-box tests were undertaken on intact and remoulded
17 loess samples collected from one of the recently active slopes replicating field
18 conditions under different simplified horizontal seismic excitations. During each test,
19 the strength reduction and excess pore water pressures generated were measured as
20 the sample failed. Test results suggest that although dynamic liquefaction could have
21 occurred, a key factor was likely to have been that the loess was largely unsaturated at
22 the times of the large earthquake events.

23
24 The failure of intact loess samples in the tests was complex and variable due to the
25 highly variable geotechnical characteristics of the material. Some loess samples failed
26 rapidly as a result of dynamic liquefaction as seismic excitation generated an increase
27 in pore-water pressure, triggering rapid loss of strength and thus of shear resistance.
28 Following initial failure, pore pressure dissipated with continued seismic excitation
29 and the sample consolidated, resulting in partial shear-strength recovery. Once excess
30 pore-water pressures had dissipated, deformation continued in a critical effective
31 stress state with no further change in volume. Remoulded and weaker samples,
32 however, did not liquefy, and instead immediately reduced in volume with an
33 accompanying slower and more sustained increase in pore pressure as the sample
34 consolidated. Thereafter excess pressures dissipated and deformation continued at a
35 critical state.

35 The complex behaviour explained why, despite exceptionally strong ground shaking,
36 there was only limited displacement and lack of run-out: dynamic liquefaction was
37 unlikely to occur in the freely draining slopes. Dynamic liquefaction however
38 remained a plausible mechanism to explain loess failure in some of the low-angle toe
39 slopes, where a permanent water table was present in the loess.

40

1
2
3
4
5
6
7
8
9
10
11
12
13
14
15
16
17
18
19
20
21
22
23
24
25
26
27
28
29
30
31
32
33
34
35
36
37
38
39
40
41
42
43
44
45
46
47
48
49
50
51
52
53
54
55
56
57
58
59
60
61
62
63
64
65

41 INTRODUCTION

42 Catastrophic landslides, particularly during earthquakes, are a significant hazard due
43 to their often rapid development, long run-out and subsequent disastrous
44 consequences (Wang et al. 2014). Whilst the global extent of loess landslides is well
45 known, (e.g. Zou and Shao 1996; Wen et al. 2004; Xu et al. 2007) the mechanism
46 through which they develop during earthquakes remains to be fully understood.
47 Although it is generally accepted that a majority of earthquake-induced landslides
48 occur through liquefaction (Seed 1966), defined by Castro et al., (1982) as a condition
49 where a soil mass loses a large percentage of its shear resistance, when subject to
50 monotonic, cyclic or shock undrained loading and flows in a manner resembling a
51 liquid until the shear stresses acting on the mass are as low as the reduced friction.
52 Laboratory based testing of loose sands (e.g. McRoberts and Sladen 1992; Sasitharan
53 et al. 1993) have demonstrated that liquefaction can occur in both undrained and
54 drained conditions as a result of rapid excess pore water pressure development
55 resulting in a sudden dramatic loss in shear resistance.

56
57 In the case of loess slopes, a number of potential mechanisms have been alluded to.
58 Assessments of the 1920 Hiyuan earthquake by Varnes (1978) suggested failures
59 occurred as dry loess flows as a result of high pore air pressures (Ter-Stepanian 1998).
60 More recent studies however (Fletcher et al. 2002; Wang and Sassa 2002; Wang et al.
61 2007; Zhang et al. 2013) indicate that soils composed almost entirely of silts are
62 liquefiable. In addition more detailed geomorphological studies of landslides (e.g.
63 Zhang et al. 1995; Zhang and Sassa 1996; Zhang and Wang 2007) find that the slope
64 failures occur from sloping source areas (20°) on concave slopes and conclude that
65 the highly mobile loess landslides are activated through liquefaction.

66
67 Loess covers 10% of the land surface of the South Island of New Zealand, and is also
68 present within the southern part of the North Island. Its wind-blown depositional
69 characteristics result in sediments that can mantle steep rock slopes, and which can
70 stand in vertical faces. In February 2011, a strong, shallow earthquake occurred
71 directly beneath the loess-covered Port Hills of Christchurch, New Zealand (Fig. 1),
72 generating unusually high ground accelerations (Kaiser et al. 2012). It was part of a
73 series of earthquakes known as the 2010-11 Canterbury Earthquake sequence.
74 Following the February 2011 earthquake, 36 large landslides were mapped, of which

1 75 the majority were in fine-grained loess on the Canterbury Port Hills. A key issue that
2 76 arose early in the ensuing aftershock sequence was whether further aftershocks could
3 77 trigger more loess landslides and if so, under what circumstances might they cause
4 78 fatalities? Historical data for New Zealand indicated loess landslide fatalities during
5 79 heavy rain, but not during strong earthquakes. International precedent is different:
6 80 about 4000 people were killed in July 1949 in the earthquake-triggered Yasman valley
7 81 loess flow in the vicinity of Khait, Tajikistan (Evans et al. 2009). The earthquake -
8 82 triggered numerous loess landslides and killed about 7200 people in total. A key
9 83 factor there appears to have been that the loess was wet at the time of the earthquake,
10 84 and landslide run-out was across saturated ground (Evans et al. 2009).

11 85
12 86 Despite advances in understanding the mechanisms of loess landslide development
13 87 (e.g. Xu et al. 2007), further data are required on the performance of both intact and
14 88 remoulded loess during seismic excitation. This study sought to explore this issue
15 89 through an experimental investigation of loess behaviour during seismic excitation
16 90 using samples from the Canterbury Port Hills. We took samples of intact primary
17 91 airfall loess from near the Maffey's Road loess landslide (Massey et al. 2013), which
18 92 moved about 0.7 m during the Canterbury Earthquake sequence without catastrophic
19 93 failure leading to long run-out. The samples were tested in a Dynamic Back Pressured
20 94 Shearbox (DBPSB, www.gdsinstruments.com, accessed 14 January 2015). The
21 95 DBPSB is based on a standard direct-shear device, modified to allow the
22 96 measurement and control of pore pressure and dynamic application of normal and
23 97 shear stresses (Brain, et al. 2015). This device can be used for static and dynamic
24 98 direct-shear testing of intact or remoulded soils with control of pore pressure to allow
25 99 realistic landslide mechanisms to be simulated in the laboratory. Using this device we
26 100 sought to explore whether earthquake shaking could induce loess slope failures by
27 101 liquefaction as defined by Castro et al (1982), and why during the 2010-2011
28 102 earthquake sequence it did not.

29 103 30 104 THE PORT HILLS AND THEIR LOESS CHARACTERISTICS

31 105 The Christchurch Port Hills (hereafter referred to simply as the Port Hills) are located
32 106 between the city of Christchurch and the port of Lyttelton on the South Island of New
33 107 Zealand (Fig. 1). The Port Hills form the northern sector of the eroded extinct
34 108 Lyttelton basalt volcano and the rocks belonging to the Miocene Lyttelton Volcanics

109 Group. These rocks comprise layers of hard, jointed, basalt and trachy-basalt lava
110 flows cut by dykes, and interbedded with breccia (scoria) and epiclastic deposits
111 comprising agglomerate (coarse angular gravel), compact sandy tuff (ash and re-
112 worked ash), fluvial deposits (poorly sorted conglomerates and coarse sandstones),
113 and ancient buried soils.

114

115 The eroded volcano is mantled by soils predominantly derived from wind-blown sand
116 and silt (loess), of the Banks Peninsula Loess (Brown and Weeber, 1992). This loess
117 forms a predominantly thick sheet (>1 m) over Banks Peninsular (Fig. 1). At least
118 four periods of loess deposition, separated by periods of relative quiescence, and soil
119 formation are recognised in the most complete sections of the Banks peninsula
120 (Griffiths, 1973). It is a relatively cohesive, silt-dominated soil with only minor clay
121 mineral content. Its mechanical properties when wet have been much studied (e.g.
122 Bell et al. 1986; Bell and Trangmar 1987; McDowell 1989; Goldwater 1990; Yetton
123 1992; Carey et al. 2014). These studies indicate regional differences between loess
124 from northern and southern Banks Peninsular, but little variation locally around the
125 Port Hills.

126

127 The Canterbury Plains to the west of Banks Peninsula are extensive alluvial fans and
128 the likely dominant source of the loess. The prevailing westerly winds access silt and
129 fine sand from the braided channels of the rivers crossing the Canterbury Plains The
130 river sediments are derived from mainly quartzofeldspathic greywacke sandstone and
131 argillite of the Southern Alps. During sea level stands of up to 120 m below current
132 level the fans extended east of Banks Peninsular and frequent easterly winds could
133 also deposit loess in the Port Hills (Raeside 1964). Although there is much primary
134 air-fall deposited loess, there is also much colluvially reworked loess (Griffiths,
135 1973), which is the expected outcome of air-fall deposition in a humid environment.

136

137 The surface morphology of Banks Peninsular is one of a deeply dissected volcano
138 'softened' by a mantle of loess that is thin and discontinuous at higher altitudes, but
139 forming a thick layer (up to 20 m) that almost totally blankets the lower slopes and
140 spurs. Major historical colluvial activity has been episodic, limited to wet periods,
141 with triggering of shallow slide/flows and extensive slope wash by high intensity
142 rainstorms (Bell and Trangmar 1987).

143

144 THE CANTERBURY EARTHQUAKE SEQUENCE

145 The Canterbury earthquake sequence started on 4 September 2010 with an M_w 7.1
146 earthquake 40 km west of Christchurch at Darfield (Bannister and Glenhill 2012)
147 (Fig. 1). The event was followed on 22 February 2011 by the M_w 6.1 Christchurch
148 earthquake, which was centred 6 km southeast of the city centre beneath the northern
149 edge of the Port Hills. This well recorded event had maximum vertical peak ground
150 accelerations of 2.2 g (Kaiser et al. 2012). It triggered many landslides, mainly
151 rockfalls and debris avalanches, over an area of 65 km² of the Port Hills (Dellow et al.
152 2011). In the following 10 months there were over 85 $M_w \geq 4.0$ aftershocks with
153 epicentres close to or immediately below the Port Hills (Gledhill et al. 2011; Kaiser et
154 al. 2012; Ristau et al. 2013), some of which triggered further landslides.

155

156 Each identified earthquake-induced mass movement was classified by failure type
157 (Massey et al. 2014), primarily inferred from the materials and the movement style,
158 based broadly on the landslide classification scheme of Cruden and Varnes (1996).
159 Whilst many mass movement types were observed within the Port Hills, the majority
160 of landslides within the loess were of two main types.

161

162 Failure type 1 comprised landslides from loess slopes overlying bedrock (Fig 2a). In
163 some cases these failures were entirely within the loess and were not influenced by
164 the underlying bedrock (Fig 2b). In other cases, failure occurred at the interface
165 between the loess / loess colluvium and the rock beneath (Fig 2c). These failures
166 typically occurred where thick (> 5 m) loess mantled the tops of steep slopes (cliffs –
167 typically steeper than 60°) exposing volcanic rock. Despite significant deformation of
168 these slopes, these failures did not develop into long run-out loess debris avalanches
169 or flows as has been experienced in other earthquake events (Evans et al. 2009).
170 Instead these failures typically generated a series of tension cracks with significant
171 cumulative vertical (up to 1 m) and horizontal displacement (up to 5m) in the loess
172 mantled over the rock slope, causing local damage only.

173

174 Failure type 2 comprised large shallow slope slides or ‘toe slumps’ within the gentle
175 valley-bottom loess slopes (Fig 2d). These failures mainly occurred in locations where

176 low angle (typically less than 25°) slopes in the Port Hills graded into flatter areas of
177 the valley bottom, with permanent relatively high water tables (Fig 2e).
178 Displacements at these sites were generally less than 1.5 m and commonly resulted in
179 laterally extensive linear zones of property-damaging cracking and extension at the
180 crest of the failure. The main body of the landslide downslope was simply translated
181 with limited damage to property. At the toe was another zone of extensive property
182 damage, but from compression. The toe area also showed evidence of water saturation
183 (water springs, ponding and sand boils), which was not merely from broken service
184 pipes.

185
186 Both types caused much property damage, but neither was associated with fatalities.
187 This stood in marked contrast with the historical record, where there have been three
188 deaths from rainfall-induced loess-on-rock failures recorded on Banks Peninsula,
189 however, these did not occur in the Port Hills (Eileen McSaveney pers comm, 2015).
190 Prior to the earthquake sequence, stability of the loess during rain had been a major
191 focus of geotechnical investigation.

192 193 MAFFEYS ROAD MASS MOVEMENT AREA

194 One of the many mass movement sites identified in the loess mantled slopes of the
195 Port Hills was at Maffey's Road (Fig 3). The site morphology indicated that the slope
196 formed as an embayment along a now-abandoned sea cliff, with localised evidence of
197 past landslide scars. The slopes above the cliff are, for the most part, mantled by loess.

198
199 As noted earlier, previous studies suggested that one site was as good as any other site
200 for sampling loess in the Port Hills. Hence, ease of access for retrieval of heavy intact
201 samples and the known history of the site were the primary reasons for selecting the
202 Maffey Road site for sampling. The test results, however, revealed a high variability
203 of behaviour of intact samples from that one site, which may not have been evident if
204 we had chosen to sample from many sites.

205
206 Prior to the earthquake sequence there had been no large-scale slope deformation at
207 Maffey's Road since first European settlement (ca. 1840 AD); although a small earth
208 flow in the loess, caused by water from a pipe break, occurred in 2011 (Yetton and

1
2
3
4
5
6
7
8
9
10
11
12
13
14
15
16
17
18
19
20
21
22
23
24
25
26
27
28
29
30
31
32
33
34
35
36
37
38
39
40
41
42
43
44
45
46
47
48
49
50
51
52
53
54
55
56
57
58
59
60
61
62
63
64
65

209 Engel 2014). No damage was reported at Maffeys Road following the 4 September
210 2010 earthquake, but cracks and other damage were found after the earthquakes of 22
211 February 2011 (Yetton and Engel 2014; Massey et al. 2014). The cracks indicated
212 permanent slope displacement of about 0.5 m (Fig 2). Further small amounts of
213 downslope movement were found following earthquakes on 13 June 2011 (c. 0.1 m)
214 and 22 December 2011 (c. 0.01 m) (Massey et al. 2014).

215
216 A conceptual ground model (Fig 4) suggests that the loess mantling the Maffeys Road
217 slope is similar to that found across much of the Port Hills (Massey et al. 2014). A
218 thin layer of variable thickness of clayey silty gravel colluvium underlies the loess
219 across much of the site. The colluvium is underlain by massive volcanic breccia with
220 several flows of basalt lava. The lava breccia is weak to very weak with variable rock
221 quality designation as low as 15% (Yetton and Engle 2014). An interpretation of the
222 bedrock surface suggests an overall dip of approximately 16° towards the south-east;
223 approximately coincident with the surface slope aspect (Massey et al. 2014). There is
224 no evidence of instability in the units below the interface with the loess at this site.

225 226 METHODOLOGY

227 A suite of laboratory tests was used to determine the geotechnical characteristics of
228 the loess from the Maffeys Road site. The experiments comprised a series of standard
229 multi-stage loaded torsional ring shear tests on remoulded samples together with
230 direct shear tests on both remoulded and undisturbed samples to establish
231 representative field-stress conditions designed to simulate horizontal seismic
232 excitation in a saturated loess slope.

233
234 Samples were collected as large intact blocks from the exposed loess cliffs at the
235 Maffeys Road site (Fig 3). Each block was hand excavated from the cliff to avoid
236 disturbance and, then wrapped to maintain natural moisture content before being
237 boxed to avoid damage during transport. Standard soil classification tests were
238 undertaken to establish the loess physical properties (Table 1 and Fig. 5). Particle-size
239 analyses (Fig. 5) confirms that that the loess is fine grained comprising of
240 approximately 50% Clay and 40 - 45% silt with the remaining fraction consisting
241 mostly fine and medium grained sand. The natural moisture content was measured at
242 9.1% (Table 1) and a plastic limit of 16%; a liquid limit of 25% and plasticity index

1
2
3
4
5
6
7
8
9
10
11
12
13
14
15
16
17
18
19
20
21
22
23
24
25
26
27
28
29
30
31
32
33
34
35
36
37
38
39
40
41
42
43
44
45
46
47
48
49
50
51
52
53
54
55
56
57
58
59
60
61
62
63
64
65

243 of 9% indicating it lies at the boundary between a low plasticity silt and clay (defined
244 in accordance with BS5930, 1981). These values are within the typical ranges
245 previously measured for loess within the Port Hills (Yetton, 1986; Glassey, 1986;
246 Tehrani, 1988; McDowell, 1989).

247
248 Ring-shear tests on remoulded loess samples were undertaken using a Bromhead-type
249 Wykeham Farrance ring shearbox. During testing, the normal and shear loads, and the
250 displacement, were recorded using a Picologger ADC24 data logger.

251
252 Ring-shear specimens were prepared from the loess sample blocks and each sample
253 was prepared tested following standardised procedures (BSI, 1990). Consolidation
254 was carried out incrementally through the addition of weights to the 10:1 lever ratio
255 loading arm. Following consolidation, a slow shear rate of 0.0178 mm/min was
256 applied to ensure no excess pore pressure was generated during shear.

257
258 Shearing was multi-stage at three normal stresses (154, 276 and 521 kPa); shearing at
259 each normal stress was continued until a constant shear stress was observed. In each
260 case, primary consolidation was completed before shearing was initiated. After the
261 shear phase at the maximum normal stress (521 kPa), the normal stress was reduced
262 back to 154 kPa before shearing was repeated to obtain a comparison with initial
263 loading.

264
265 A further series of both standard and dynamic soil tests was carried out under direct
266 shear using a Dynamic Back-Pressured Shearbox (DBPSB) constructed by GDS
267 Instruments Ltd. The DBPSB provides the opportunity to carry out both static and
268 dynamic direct shear testing on soils whilst controlling back pressure and measuring
269 pore water pressure in the sample. The DBPSB is conceptually based on a standard
270 direct shear device, but modified to allow the measurement and control of pore
271 pressures and dynamic application of normal stress and shear stress (Fig. 6).

272
273 The apparatus, which can function as both a conventional direct shear and back
274 pressured shear machine, uses 100 mm x 100 mm x 20 mm samples. The machine
275 provides both static and dynamic control of: horizontal (shear) and axial (normal)

1 276 force and displacement; total stress; and effective stress. Sample pore water pressure
2 277 can be monitored.

3 278

4 279 The DBPSB comprises both an upper and lower section of the sample vessel which is
5 280 assembled using connecting screws. The lower section of the sample vessel contains a
6 281 porous plate that is placed into a lower circular recess. Soil samples are placed into
7 282 the sample vessel with filter papers of the same dimensions placed on the upper and
8 283 lower sides of the sample. The sample vessel is then securely mounted in a sealed
9 284 pressure vessel, an upper porous plate is placed on top of the specimen and vertical
10 285 spacer is placed on the sample vessel after the connection screws have been removed.
11 286 The vessel is sealed by the upper section of the DBSB apparatus using fastening
12 287 screws. The load cell fits directly onto the upper porous plate. A vertical rod is
13 288 connected to the apparatus and can apply a normal load to the sample, which is
14 289 controlled by a hydraulic pressure controller.

15 290

16 291 The pressure vessel is flooded with de-aired water, and fluid pressure within the
17 292 chamber is measured using two transducers, one mounted on a line that terminates
18 293 adjacent to the sample, and the other on the fluid pressure control line.

19 294

20 295 The system is controlled and data logged using the GDSLAB control software,
21 296 designed and developed by GDS, which runs on a standard PC.

22 297

23 298 The DBPSB was initially used for a standard shear-box test on an undisturbed sample
24 299 (SB1) at a confining pressure of 148 kPa. To replicate the testing conditions on the
25 300 remoulded ring shear tests, the sample was initially saturated by filling the shear box
26 301 cell with water and then applying staged normal loads of 154, 276 and 521 kPa. Once
27 302 consolidation was achieved a standard shear test was undertaken at a strain rate of
28 303 0.01 mm/min.

29 304

30 305 Other undisturbed loess samples were initially saturated in the DBSB to replicate
31 306 samples below the groundwater table. Pore air pressures were eliminated by flushing
32 307 the sample with carbon dioxide at a slow, controlled rate, before de-aired water was
33 308 flushed into both the shear box and sample to fill the pore air voids and ensure each
34 309 sample was fully saturated. Once saturation was complete, the back pressure and

1
2
3
4
5
6
7
8
9
10
11
12
13
14
15
16
17
18
19
20
21
22
23
24
25
26
27
28
29
30
31
32
33
34
35
36
37
38
39
40
41
42
43
44
45
46
47
48
49
50
51
52
53
54
55
56
57
58
59
60
61
62
63
64
65

1
2
3
4
5
6
7
8
9
10
11
12
13
14
15
16
17
18
19
20
21
22
23
24
25
26
27
28
29
30
31
32
33
34
35
36
37
38
39
40
41
42
43
44
45
46
47
48
49
50
51
52
53
54
55
56
57
58
59
60
61
62
63
64
65

310 normal stress were simultaneously progressively ramped to 240 kPa and 250 kPa over
311 120 minutes to dissolve any remaining carbon dioxide into solution in the sample.
312 During this period the normal stress was always kept 10 kPa higher than the back
313 pressure to maintain a small positive normal effective stress and to prevent sample
314 swelling during the saturation process.

315
316 Sample consolidation was undertaken by applying a normal stress, as in an oedometer
317 or standard direct shear test. A normal effective stress of 150 kPa was applied, to
318 replicate field conditions, by reducing back pressure to 100 kPa whilst holding a total
319 normal stress of 250 kPa. Normal stress was controlled by maintaining the normal
320 load applied through a feedback-controlled actuator that permits the control of stress
321 or displacement / strain.

322
323 On successful completion of the consolidation stage of the test, an initial stage of
324 direct shear was undertaken. In each test, the shear force was applied to the sample at
325 a strain rate of 0.01 mm/min. The sample was subjected to this shear stage until a
326 predetermined shear strain of 0.5% was reached, at which point the shear force was
327 held constant for up to 12 hours to allow creep to effectively cease.

328
329 Following the initial shear stage, seven samples (DYN1 to DYN7) were subject to a
330 drained, strain-controlled, dynamic shear phase (Table 2). In each test, samples were
331 subject to a displacement-controlled horizontal shear of +/- 0.5mm at a constant
332 normal stress of 400 kPa and a constant back pressure of 100 kPa. Each test was
333 undertaken under displacement control and so strain accumulation could not be
334 analysed; instead the shear stress and pore-water pressure characteristics measured
335 during the dynamic tests were used to determine the nature of each stress path to
336 failure.

337
338 To analyse the impacts of the frequency of seismic excitation, four samples (DYN1 to
339 DYN4) were subjected to dynamic shear phases for a period of 60 seconds at
340 frequencies ranging from 1 Hz (60 dynamic cycles) to 4 Hz (240 dynamic cycles). As
341 each test was subject to displacement- controlled shear, the key measured parameter is
342 shear strength. To assess the impact of repeated dynamic cycles, one sample (DYN5)
343 was subjected to 10 individual dynamic shear stages at a frequency of 2 Hz for a

344 period of 1 minute each, at intervals of 10 minutes. One test (DYN6) was undertaken
345 to assess the impact of long-duration seismic excitation on the shear surface. During
346 this test, the sample was subject to a 2 Hz dynamic shear phase for a period of 10
347 minutes. The same test was then conducted on a remoulded loess sample (DYN7) to
348 assess the variability in intact and remoulded behaviour.

349

350 RESULTS

351 A consolidation curve for the multi-stage ring-shear test (RS1) was constructed from
352 incremental loadings to a final initial confining pressure of 154 kPa (Fig 7 a). As
353 anticipated, the sample experienced an increase in vertical strain through time to 4.6
354 %. Incremental loading was also used to consolidate sample SB1 in the DPBSB (Fig 7
355 b) which increased vertical strain of 9.7%. Sample SB2 was subject to a single
356 loading phase and showed similar consolidation behaviour with an increase in vertical
357 strain of 8.6% (Fig 7 b).

358

359 Consolidation curves of the DBPSB tests were constructed at a normal effective stress
360 of 150 kPa. The results show some variability in behaviour between samples, with a
361 trend of increasing vertical strain through time (Fig 7 c). DBPSB samples
362 consolidated to vertical strains of between 5.5% and 6.5% at 150 kPa.

363

364 The shear behaviour in the ring shear test (RS1) showed consistent ductile behaviour
365 during each loading cycle, with shear stress increasing to a near constant stress at each
366 stage (Fig 8 a). Both the undrained and drained shear-box tests carried out in the
367 DBPSB also showed (Fig 8 b) similar behaviour to the ring-shear test. In both tests,
368 shear stress began to plateau at approximately 10% shear strain, although higher
369 stresses were measured in the drained test. In both tests, a slight increase in shear
370 stress was then observed with increasing strain, although this change in stress was
371 more significant in undrained shear test (SB2) when a constant back pressure was
372 maintained throughout shear.

373

374 The multi-staged ring-shear tests were used to calculate Mohr-Coulomb parameters
375 and indicated a drained angle of internal friction of 27° and cohesion of 6 kPa, which
376 was consistent within error with both the standard direct drained and undrained shear
377 tests in the DBPSB (Fig 8 c). These strength-envelope characteristics lay within the

1
2
3
4
5
6
7
8
9
10
11
12
13
14
15
16
17
18
19
20
21
22
23
24
25
26
27
28
29
30
31
32
33
34
35
36
37
38
39
40
41
42
43
44
45
46
47
48
49
50
51
52
53
54
55
56
57
58
59
60
61
62
63
64
65

378 range of other values calculated using direct-shear and ring-shear tests for other loess
379 from near Christchurch (Bell et al. 1986; Goldwater 1990; Carey et al. 2014).

380
381 The initial shear stage indicated significant variation in strength characteristics
382 between samples (Fig 9 a), due to micro-scale variability in the structure of the loess.
383 Whilst samples DYN5 and DYN6 achieved similar shear stress of 40 and 45 kPa
384 respectively at 2.5 % shear strain, all other samples demonstrated shear stresses
385 ranging from 25 kPa to 33 kPa at the same shear-strain level. Sample DYN1
386 underwent a loss of shear stress at the end of the test when 2.5 % strain was achieved,
387 reducing to 22 kPa whilst strain was held constant. Each sample generated a relatively
388 consistent pore-water pressure during the initial shear stage (Fig 9 b).

389
390 The horizontal displacement was accurately controlled by the DNBPSB throughout
391 each dynamic test (Fig 10 a) and subsequently the change reduction in shear stress
392 (Fig 10 b), development of pore-water pressure (Fig 10 c) and the relationship
393 between shear strain and shear stress were recorded throughout each test. Given the
394 complexity of behaviour, we present the results of each dynamic test in terms of pore-
395 water response, shear stress and normal effective stress by plotting these values at
396 peak shear stress measured during each dynamic cycle (Fig 11).

397
398 In the first set of dynamic experiments (DYN1 – DYN4), shear stress was applied at a
399 range of frequencies. The response of the samples was variable, with the 1-Hz
400 (DYN1) and 3-Hz (DYN3) samples displaying liquefaction and resultant high pore-
401 water pressures (Fig 11 a). In these tests, the stress paths reached the conventional
402 strength envelope in the first cycle, and then progressively weakened as excess pore
403 pressure was generated. Eventually, pore-water pressures peaked and started to
404 decline (Fig 11 b), which permitted the samples to strengthen, but in this case defining
405 a second envelope with zero cohesion and a lower effective angle of internal friction.

406
407 The 2-Hz (DYN2) and 4-Hz (DYN4) samples, which were observed to be the weakest
408 samples during the initial shear phase, showed slightly different behaviour. These
409 samples also reached the conventional strength envelope in the first cycle, but then
410 rapidly weakened. Sample DYN2 demonstrated behaviour in the early stage of the test
411 that was similar to the liquefaction seen in samples DYN1 and DYN3, but a lower

1
2
3
4
5
6
7
8
9
10
11
12
13
14
15
16
17
18
19
20
21
22
23
24
25
26
27
28
29
30
31
32
33
34
35
36
37
38
39
40
41
42
43
44
45
46
47
48
49
50
51
52
53
54
55
56
57
58
59
60
61
62
63
64
65

412 strength envelope appears to have been defined (Fig 11 a). Sample DYN4 also
413 generated high pore-water pressure, although significantly more cycles were required
414 to reach a peak pressure. As a consequence, liquefaction did not occur. It was
415 noticeable that the pore pressure response was variable between the tests, for example
416 sample DYN4 sustained a peak pore pressure whilst the other tests showed rapid pore
417 pressure dissipation (Fig 11 b).

418
419 To further explore this behaviour, a test was conducted in which a sample (DYN6)
420 was subjected to 2-Hz dynamic shear stress for 600 seconds (i.e. for a duration that
421 was an order of magnitude longer than that in the former series of tests). In this case,
422 the sample also showed liquefaction and progressive weakening along the
423 conventional failure envelope (Fig 12 a), similar to samples DYN1 and DYN3. By the
424 end of the experiments, the excess pore pressure had fully dissipated (Fig 12 b).

425
426 In a further experiment, sample (DYN5) was subjected to 10 discrete phases of
427 dynamic shear at 2-Hz, which in sum amounted to the same number of cycles as in
428 test (DYN6). As before, the sample displayed liquefaction in the first 60 cycles (Fig
429 13 a). In the second phase of 60 cycles, the sample attained a peak shear stress that
430 was significantly lower than in the first phase, and then weakened through
431 liquefaction and the generation of excess pore pressure. However, in each subsequent
432 cycle thereafter, the sample reached successively higher peak strengths and a higher
433 final strength value. By cycle 10, the sample no longer generated excess pore pressure
434 and reached a peak strength that was greater than the original peak strength value (Fig
435 13 b), suggesting sample strengthening as a result of densification.

436
437 One test was conducted on a remoulded sample (DYN7). This sample reached the
438 peak-strength envelope in the first cycle (Fig 14 a), but then rapidly weakened without
439 generating much increased pore pressure (Fig 14 b) in a style similar to sample
440 DYN4. In subsequent cycles, the sample generated excess pore pressure with very
441 little reduction in shear stress. Later in the test, the excess pore pressure dissipated;
442 the inflection point appeared to coincide with the conventional peak-strength
443 envelope. The sample weakened slightly as pore pressure dissipated.

444
445 DISCUSSION

1
2
3
4
5
6
7
8
9
10
11
12
13
14
15
16
17
18
19
20
21
22
23
24
25
446 The loess samples tested in the suite of drained dynamic shear experiments showed
447 somewhat variable behaviour, indicating complex mechanisms of deformation.
448 Dynamic liquefaction was observed in some of the tests. In these cases, the
449 conventional failure envelope was reached during the first dynamic cycle (Fig 15 a),
450 and subsequent cycles led to a rapid development of excess pore pressure and a
451 corresponding decrease in shear strength at a nearly constant sample volume (Fig 15
452 b), until the sample shear surface underwent dynamic liquefaction, causing the shear
453 strength of the sample to drop below the conventional strength envelope. During this
454 phase of deformation, the sample strength was no longer controlled by the frictional
455 strength of the loess. During the collapse and flow phase, the pore water pressures
456 dissipated whilst the sample volume continued to reduce, suggesting densification of
457 the shear surface. As pore pressure dissipated, samples regained shear strength,
458 although shear stresses remained significantly lower than the conventional failure
459 envelope.

26
27
28
29
30
31
32
460
461 Intact samples subjected to many cycles (DYN6) of dynamic shear appeared to reach
462 an ultimate critical state. Samples in this state no longer accumulated vertical strain
463 and therefore deformed at constant volume (Fig 16).

33
34
35
36
37
38
39
40
41
42
43
44
45
46
47
48
49
50
51
52
464
465 Similar failure mechanisms were observed in a series of undrained and drained
466 triaxial tests on sands (Sladen et al. 1985; Sasitharan et al. 1993). These studies
467 concluded that liquefaction failures occur along a collapse surface in three
468 dimensional void ratio - shear stress - normal stress space. This collapse concept was
469 argued to be fundamentally an extension of critical state soil mechanics (Sladen et al.
470 1985). In addition, more recent laboratory studies (Wang et al. 2014) comprising
471 undrained triaxial compression and ring-shear tests on remoulded loess demonstrate
472 that water-saturated loess is highly susceptible to liquefaction and flow failure, whilst
473 fast shear tests on dried, air-saturated loess generated only small pore air pressures
474 and no significant reduction in shear resistance.

53
54
55
56
57
58
59
60
61
62
63
64
65
475
476 The weakest samples at 2 Hz and 4 Hz (DYN2, DYN4) and the remoulded 2-Hz 10
477 min (DYN7) tests showed different behaviour. In these tests, dynamic shear caused a
478 more immediate decrease in sample volume (Fig 17 a). We hypothesise that because
479 these samples were disturbed, their permeability, and therefore their ability to drain

1 480 during dynamic shear may have been greater. As a consequence, excess pore water
2 481 pressures were less likely to be generated at constant volume during the early stages
3 482 of the test. In these cases, the samples show post-failure pore pressure generation,
4 483 without further weakening. We further hypothesise that the dynamic shear and more
5 484 gradual rise of pore pressures occurred as the damaged sample were able to drain
6 485 faster than the intact samples. As a consequence, liquefaction and collapse did not
7 486 occur, but instead the material deformed through a flow-type mechanism until pore
8 487 pressures dissipated through sample densification (Fig 17 b). In the case of the
9 488 remoulded sample (DYN7) deformation at the end of the test reached a constant
10 489 critical state (Fig 16). In these experiments it should be noted that the sample was
11 490 returned to the same value of shear strain at the end of each cycle, such that a stress –
12 491 strain curve could not be generated.

13 492
14 493 We noted the different behaviour observed between the remoulded sample subjected
15 494 to 600 seconds of dynamic shear stress at 2 Hz (DYN7) and that subjected to ten
16 495 cycles of dynamic excitation (DYN5), each lasting 30 seconds, also at 2 Hz. At the
17 496 end of the tests, both samples had been subjected 600 cycles at the same frequency (2
18 497 Hz). However, in sample DYN5, the excess pore pressure generated by the dynamic
19 498 shear stress was allowed to dissipate prior to the start of the next cycle (Fig 18 a). In
20 499 this case, the sample showed the same dynamic liquefaction behaviour during the first
21 500 dynamic cycle as was observed in other intact sample tests (Fig 13 a). Subsequent
22 501 cycles, however, showed an increase in density and as consequence pore water
23 502 pressure and sample volume progressively reduced with each cycle (Figure 18 a).
24 503 Thus, whilst a similar failure envelope was observed during the second cycle in
25 504 sample DYN5 and the remoulded sample DYN7, indicating that liquefaction could no
26 505 longer occur, repeat cycles successively strengthened sample DYN5 back toward the
27 506 conventional failure envelope (Fig 18 b). These results suggested that successive
28 507 periods of earthquake shaking may act to consolidate the loess, making liquefaction
29 508 and instability less likely in future seismic events.

30 509 31 510 CONCLUSION

32 511 Mechanisms of failure in loess slopes during seismic excitation were studied through
33 512 a series of dynamic shear tests using a newly developed dynamic back-pressured
34 513 shear box (Model DBPSB of GDS Ltd). This new machine allows laboratory

1
2
3
4
5
6
7
8
9
10
11
12
13
14
15
16
17
18
19
20
21
22
23
24
25
26
27
28
29
30
31
32
33
34
35
36
37
38
39
40
41
42
43
44
45
46
47
48
49
50
51
52
53
54
55
56
57
58
59
60
61
62
63
64
65

514 simulation of complex hillslope environments to study the nature and cause of
515 earthquake-induced landslides. The study demonstrated that a saturated intact loess
516 slope can fail during seismic excitation as a result of dynamic liquefaction of the shear
517 surface (Sladen et al.1985).

518
519 In a saturated intact loess slope, sufficient dynamic shear may collapse the shear zone,
520 creating a very rapid increase in pore water and rapid reduction in shear strength.
521 Following failure, these excess pore pressures rapidly dissipate as water drains away.
522 As a consequence, the shear zone consolidates and the shear strength increases until
523 reaching a critical state. The final critical state during seismic excitation may have
524 lower shear strength than the conventional residual strength envelope. This rapid
525 reduction in mean normal effective stress is capable of generating rapid failures of
526 slopes during earthquakes, as has been observed in a number of previous events (e.g.
527 Wang et al. 2014).

528
529 In some instances, however, loess slopes with sufficiently small pore spaces, such as
530 previously disturbed slopes or slopes in fine-grained or dense loess deposits can
531 rapidly weaken during seismic excitation without failing through dynamic
532 liquefaction. In these slopes, dynamic shear rapidly reduces shear strength but excess
533 pore-water pressure is generated at a slower rate. Pore water pressures subsequently
534 dissipate, allowing strengthening until reaching a critical state. Again, this final state
535 during seismic excitation has lower shear strength than the conventional residual
536 strength envelope. Whilst the reduction in strength and increase in pore pressure are
537 likely to result in slope failure, the displacement rate of such failures may be
538 significantly slower than observed from dynamic liquefaction.

539
540 Repeat cycles of dynamic excitation where excess pore pressure could dissipate
541 between each dynamic stage suggest that following dynamic liquefaction, each
542 successive phase of dynamic shear further consolidates the shear zone. As a
543 consequence, pore-pressure generation is lower during successive cycles and both the
544 dynamic shear strength and conventional strength envelope progressively increase.
545 The results suggest that once initial failure of a loess slope occurs, successive
546 earthquakes are unlikely to reduce the stability further and may indeed strengthen the
547 slope.

548

1
2 549 Although exceptional levels of ground shaking occurred during the Canterbury
3
4 550 earthquake sequence, the results suggest that dynamic liquefaction probably did not
5
6 551 occur in the type 1 loess landslides such as at Maffeys Road, which underwent
7
8 552 relatively small displacements (e.g. total displacements in the order of millimetres)
9
10 553 with little run-out. The geological characteristics of these slopes suggest they are
11
12 554 relatively free-draining loess deposits that were relatively dry when seismically
13
14 555 excited. As a consequence, if any collapse occurred, it did not develop sufficient
15
16 556 excess pore pressure to drive dynamic liquefaction.

557

17
18 558 Failures seated in the type 2 loess landslides, however, where a water table was
19
20 559 present in the loess, are likely to be susceptible to dynamic liquefaction. In these
21
22 560 slopes, movement occurred at a variety of very low slope angles (approximately 15°)
23
24 561 in loessial materials with angles of internal friction of about 30°. Their movement
25
26 562 locally caused much damage to structures where there was surface deformation
27
28 563 (shear, compression and extension), but much motion was as a series of non-
29
30 564 deforming rafts.. Still these landslides had only limited total displacement, with most
31
32 565 of it during the strong seismic activation, with little post-seismic creep.

566

33
34 567 ACKNOWLEDGMENT

35
36 568 The authors thank Chris Massey, Mark Yetton for information and advice.
37
38 569 Christchurch City Council facilitated site access and provided data from boreholes
39
40 570 and mapping studies. Zane Bruce and Mark Yetton assisted in the field sampling.
41
42 571 Stuart Read and Peter Barker are thanked for their support during the laboratory
43
44 572 testing and analysis phase which was undertaken within the GNS rock and soil
45
46 573 mechanics laboratory. We also thank our GNS Science colleagues Will Ries and
47
48 574 Darren D’Cruz who prepared the figures and Phil Glassey for his constructive review
49
50 575 of an earlier draft of this manuscript. The research has in part been supported by the
51
52 576 GNS Science Strategic Development Fund, the GNS direct crown funded Landslide
53
54 577 Hazards Programme and by the NERC/ESRC Increasing Resilience to Natural
55
56 578 Hazards programme under the Earthquakes Without Frontiers project, grant reference
57
58 579 NE/J01995X/1 and NERC/Newton Fund grant NE/N000315.REFERENCES

1
2
3
4
5
6
7
8
9
10
11
12
13
14
15
16
17
18
19
20
21
22
23
24
25
26
27
28
29
30
31
32
33
34
35
36
37
38
39
40
41
42
43
44
45
46
47
48
49
50
51
52
53
54
55
56
57
58
59
60
61
62
63
64
65

580 Bannister SC, and Gledhill KR (2012) Evolution of the 2010-2012 Canterbury
581 earthquake sequence. *New Zealand Journal of Geology and Geophysics*, 55(3): 295-
582 304.

583 Bell DH, Glassey PJ, Yetton MD (1986) Chemical stabilisation of dispersive loessical
584 soils, Banks Peninsula, Canterbury, New Zealand. *Proceedings of the 5th*
585 *International Congress of the International Engineering Geological Society*, 1: 2193-
586 2208

587 Bell DH, Trangmar BB (1987) Regolith materials and erosion processes on the Port
588 Hills, Christchurch, New Zealand: *Fifth International Symposium and Field*
589 *Workshop on Landslides*. Lausanne, A.A. Balkema. Volume 1: 77-83.

590 Brain MJ, Rosser NJ, Sutton J, Snelling K, Tunstall N, Petley DN (2015) The effects
591 of normal and shear stress wave phasing on coseismic landslide displacement. *Journal*
592 *of Geophysical Research: Earth Surface*. 120, 1009-1022.

593 Brown LJ, Weeber JH (1992) Geology of the Christchurch urban area. Scale
594 1:25,000. *Institute of Geological & Nuclear Sciences geological map*. 1.

595 British Standards Institute (BSI) (1981) Code of Practice for Site Investigations. BS
596 5930: 1981.

597 British Standards Institute (BSI) (1990) British standard methods of test for soils for
598 civil engineering purposes. Part 1: General requirements and sample preparation. BS
599 1377: Part 1.

600 Carey JM, Misra S, Bruce Z, Barker P (2014) Canterbury Earthquakes 2010/2011 Port
601 Hills Slope Stability: Laboratory Testing Factual Report. *GNS Science Consultancy*
602 *Report*.2014/53.

603 Castro G, Enos JL, France JW, Poulos SJ (1982) Liquefaction induced by cyclic
604 loading. National Science Foundation NSF/CEE-82018.

605 Cruden DM, Varnes DJ (1996) Landslides types and processes. In: Turner AK,
606 Schuster RL (eds) *Landslides Investigation and Mitigation: Transportation Research*
607 *Board*. US National Research Council, Washington, DC, pp 36-75 Special Report
608 247.

609 Dellow G, Yetto M, Massey CI, Archibald GC, Barrell DJA, Bell D, Bruce Z,
610 Campbell A, Davies T, De Pascale G, Easton M, Forsyth PJ, Gibbons C, Glassey PJ,
611 Grant H, Green R, Hancox GT, Jongens R, Kingsbury P, Kupec J, Macafarlane D,
612 McDowell B, McKelvey B, McCahon M, McPherson I, Molloy J, Muirson J,
613 O'Hallaran M, Perrin ND, Price C, Read SAL, Traylen N, Van Dissen RJ, Villeneuve

1
2
3
4
5
6
7
8
9
10
11
12
13
14
15
16
17
18
19
20
21
22
23
24
25
26
27
28
29
30
31
32
33
34
35
36
37
38
39
40
41
42
43
44
45
46
47
48
49
50
51
52
53
54
55
56
57
58
59
60
61
62
63
64
65

614 M, Walsh I (2011) Landslides caused by the 22 February 2011 Christchurch
615 earthquake and management of landslide risk in the immediate aftermath, *Bulletin of*
616 *the New Zealand Society for Earthquake Engineering*. 44(4): 227 – 238.

617 Della Pasqua F, Massey C I, Lukovic B, Ries W, Archibald G, Heron D (2014)
618 Canterbury Earthquakes 2010/11 Port Hills Slope Stability: Risk assessment for
619 Maffey's Road. *GNS Science Consultancy Report* 2014/79.

620 Evans SG, Roberts NJ, Ischuk A, Delaney KB, Morozova GS, Tutubalina O (2009)
621 Landslides triggered by the 1949 Khait earthquake, Tajikistan, and associated loss of
622 life. *Engineering Geology*, 109 (3-4): 195 – 212.

623 Fletcher L, Hungr O, Evans SG (2002) Contrasting failure behaviour of two large
624 landslides in clay and silt. *Canadian Geotechnical Journal*, 39 (1): 46–62.

625 Glassey PJ (1986) Geotechnical Properties of Lime Stabilised Loess, Port Hills
626 Canterbury. *Unpublished MSc thesis, University of Canterbury*.

627 Gledhill K, Ristau J, Reyners M, Fry B, Holden C (2011) The Darfield (Canterbury,
628 New Zealand) Mw 7.1 earthquake of September 2010: A preliminary seismological
629 report. *Seismological Research Letters*. 82 (3), 378-386.

630 Griffiths E (1973) Loess of Banks Peninsula. *New Zealand Journal of Geology and*
631 *Geophysics*, 16: 657 - 675.

632 Kaiser A, Holden C, Beavan J, Beetham D, Benites R, Celentano A, Collett D,
633 Cousins J, Cubrinovski M, Dellow G, Denys P, Fielding E, Fry B, Gerstenberger M,
634 Langridge R, Massey C, Motagh M, Pondard N, McVerry G, Ristau J, Stirling M,
635 Thomas J, Uma SR, Zhao J (2012) The Mw 6.2 Christchurch earthquake of February
636 2011: preliminary report. *New Zealand Journal of Geology and Geophysics*, 55 (1):
637 67 - 90.

638 Massey CI, Yetton MJ, Carey JM, Lukovic B, Litchfield N, Ries W, McVerry G
639 (2013) Canterbury Earthquakes 2010/11 Port Hills Slope Stability: Stage 1 report on
640 the findings from investigations into areas of significant ground damage (assessed
641 source areas). *GNS Science Consultancy Report*, 2012/317.

642 Massey CI, Della Pasqua F, Lukovic B, Ries W, Heron D (2014) Canterbury
643 Earthquakes 2010/11 Port Hills Slope Stability: Risk assessment for Cliff Street. *GNS*
644 *Science Consultancy Report*, 2014/73.

645 Massey C, McSaveney M, Taig T, Richards L, Litchfield N, Rhoades D, McVerry G,
646 Lukovic B, Heron D, Ries W, Van Dissen R 2014. Determining rockfall risk in

1
2
3
4
5
6
7
8
9
10
11
12
13
14
15
16
17
18
19
20
21
22
23
24
25
26
27
28
29
30
31
32
33
34
35
36
37
38
39
40
41
42
43
44
45
46
47
48
49
50
51
52
53
54
55
56
57
58
59
60
61
62
63
64
65

647 Christchurch using rockfalls triggered by the 2010/2011 Canterbury earthquake
648 sequence, New Zealand. *Earthquake Spectra*, 30: 155–181.

649 McDowell BJ (1989) Site investigations for residential development on the Port Hills,
650 Christchurch, M.Sc. thesis (*unpublished*). University of Canterbury.

651 McRoberts EC, Sladen JA (1992) Observations on static and cyclic sand liquefaction
652 methodologies. *Canadian Geotechnical Journal*, 29: 605 - 665.

653 Raeside JD (1964) Loess Deposits of the South Island, New Zealand, and Soils
654 formed on them. *New Zealand Journal of Geology and Geophysics*, 7: 811 - 838.

655 Ristau J, Holden C, Kaiser AE, Williams CA, Bannister SC, Fry B (2013) The
656 Pegasus Bay aftershock sequence of the M_w 7.1 Darfield (Canterbury), New Zealand
657 earthquake. *Geophysical Journal International*, 195(1): 444 - 459.

658 Goldwater S (1990) Slope failure in loess. A detailed Investigation, Allendale, Banks
659 Peninsula. MSc Thesis (*unpublished*), University of Canterbury.

660 Runqiu H, (2009) Some catastrophic landslides since the twentieth century in the
661 southwest of China. *Landslides*, 6: 69 – 81.

662 Sasitharan S, Robertson PK, Segoo DC, Morgenstern NR (1993) Collapse behaviour of
663 sand. *Canadian Geotechnical Journal*, 30: 569 – 577.

664 Seed HB (1966) Landslides during earthquakes due to soil liquefaction. *J. Soil.*
665 *Mech. Found. Div. ASCE* 94, (5), 1055–1122.

666 Sladen JA, D'Hollender RD, Krahn J (1985) The liquefaction of sands a collapse
667 surface approach. *Canadian Geotechnical Journal*, 22(4): 564-578.

668 Tehrani BH (1988) Chemical Stabilisation of Whaka Terrace Loess. *Unpublished*
669 *MSc thesis, University of Canterbury*.

670 Ter-Stepanian G (1998) Suspension force induced landslides. Proceedings of 8th
671 Congress of IAEG, Vancouver, Canada. Balkema, Rotterdam, 3, p.1905–1912.

672 Varnes, D.J. 1978. Slope movement types and processes In: Schuster RL, Krizek RJ
673 (eds) *Landslide Analysis and Control*, National Academy Sciences, Transportation
674 Research Board Spec Rep 176:11–33.

675 Wang G, Zhang D, Furuya G, Yang J (2014) Pore-pressure generation and
676 fluidization in a loess landslide triggered by the 1920 Haiyuan earthquake, China: A
677 case study. *Engineering Geology*, 174: 36-45.

678 Wang G, Sassa K (2002) Post-failure mobility of saturated sands in undrained load
679 controlled ring shear tests. *Canadian Geotechnical Journal*, 39: 821–837.

1
2
3
4
5
6
7
8
9
10
11
12
13
14
15
16
17
18
19
20
21
22
23
24
25
26
27
28
29
30
31
32
33
34
35
36
37
38
39
40
41
42
43
44
45
46
47
48
49
50
51
52
53
54
55
56
57
58
59
60
61
62
63
64
65

680 Wang G, Sassa K, Fukuoka H, Tada T (2007) Experimental study on the shearing
681 behavior of saturated silty soils based on ring shear tests. *Journal of Geotechnical and*
682 *Geoenvironmental Engineering*. ASCE 133 (3), 319–333.

683 Xu L, Dai F, Tu X, Tham GT, Zhou Y, Iqbal J (2013) Landslides in a loess platform,
684 North-West China. *Landslides*. DOI 10.1007/s10346-013-0445-x

685 Yetton MD (1986) Investigation and Remedial Methods for Subsurface
686 Erosion Control in Banks Peninsula Loess. MSc Thesis (*Unpublished*),
687 University of Canterbury.

688 Yetton MD, (1992) Engineering geological and geotechnical factors affecting
689 development on Banks Peninsula and surrounding areas – Field guide. Bell, D.H.
690 (ed.): *Landslides – Proceedings of the Sixth International Symposium, Christchurch,*
691 *10–14 February 1992*, Rotterdam, A.A. Balkema, Vol. 2(3).

692 Yetton M, Engel M (2014) Port Hills Land Damage Studies Maffey's Road Field
693 Investigations. URS Limited report for Christchurch City Council

694 Wen B, Wang S, Wang E, Zhang J (2004) Characteristics of rapid giant landslides in
695 China. *Landslides*, 1: 247 – 261.

696 Zhang D, Sassa K (1996) Study of the mechanism of loess landslides induced by
697 earthquakes. *J. Jpn. Soc. Erosion Control Eng.* 49: 4–13 (in Japanese).

698 Zhang D, Takeuchi A, Sassa K (1995) The motion characteristics of loess landslides
699 induced by the Haiyuan earthquake in Ningxia Province, China. *J. Jpn. Landslide Soc.*
700 32 (1), 12–17 (in Japanese).

701 Zhang FY, Wang G, Kamai T, Chen WW, Zhang DX, Yang J (2013) Undrained shear
702 behaviour of loess saturated with different concentrations of sodium chloride solution.
703 *Engineering Geology*, 155, 69–79.

704 Zhang D, Wang G, (2007) Study of the 1920 Haiyuan earthquake-induced landslides
705 in loess (China). *Engineering Geology*, 94: 76–88.

706 Zou JS, Shao SM (1996) Landslides induced by Haiyuan earthquake and their
707 distribution (in Chinese). *Cont Earthquake*, 10:1–5 (in Chinese).

708

709 FIGURES

1
2 710 Figure 1. Site location of the Canterbury Port Hills New Zealand.

3
4
5 711

6 712 Figure 2. Typical loess landslide types identified during the 2010-2011 Canterbury
7 earthquake sequence (a) Morphology of Type 1 failures form loess overlying bedrock
8 713 (b) Conceptual model of Type 1 failures completely within loess (c) Conceptual
9 714 model of Type 1 failures of loess along subsurface interface (d) Morphology of Type
10 715 2 failures of loess toe slumps (e) Conceptual model of Type 2 failures of loess toe
11 716 slumps.
12 717

13
14
15
16 718

17 719 Figure 3. The Maffey's Road study site (a) Maffey's Road mass movement extent
18 based on surface deformation mapping and block sampling location (b) damage
19 720 associated with earthquake-induced ground movements at Maffey's Road and (c)
20 721 sampling of exposed loess slopes.
21 722

22
23
24
25 723

26 724 Figure 4. Maffey's Road ground model (adapted from Massey et al. 2014 and Yetton
27 and Engel 2014).
28 725

29
30
31 726

32 727 Figure 5. The particle size distribution of the loess sampled at Maffey's Road.

33
34 728

35 729 Figure 6. Schematic diagram of the Dynamic Back-Pressured Shear box testing
36 apparatus.
37 730

38
39
40 731

41 732 Figure 7. Loess consolidation characteristics (a) Multi-stage ring shear test (b)
42 Conventional drained (SB1) undrained (SB2) direct shear tests in the BPSB (c)
43 733 DBPSB testing.
44 734

45
46
47 735

48 736 Figure 8. Loess shear strength characteristics from Maffey's Road using (a) multistage
49 ring shear testing and (b) drained (SB1) and undrained (SB2) direct shear testing in
50 737 the DBPSB (c) failure envelope constructed from multi-stage ring shear test compared
51 738 to shear strength characteristics observed in the undrained and drained direct shear
52 739 tests in the DBPSB.
53 740

54
55
56
57 741
58
59
60
61
62
63
64
65

1
2
3
4
5
6
7
8
9
10
11
12
13
14
15
16
17
18
19
20
21
22
23
24
25
26
27
28
29
30
31
32
33
34
35
36
37
38
39
40
41
42
43
44
45
46
47
48
49
50
51
52
53
54
55
56
57
58
59
60
61
62
63
64
65

742 Figure 9. Initial shear stage characteristics of DBPSB testing (a) shear stress against
743 strain and (b) Pore water pressure against shear strain.

744
745 Figure 10. Sample DYN2 dynamic strain controlled shear results (a) horizontal
746 displacement against time (b) shear stress against time (c) pore water pressure against
747 time (d) shear strain against shear stress.

748
749 Figure 11. Dynamic shear stage of testing at frequencies of 1, 2, 3 and 4 Hz for a
750 duration of 1 minute (a) pore water pressure against cycle number and (b) shear stress
751 against normal effective stress.

752
753 Figure 12. Dynamic shear stage of testing at a frequency of 2 Hz for a duration of 10
754 minutes on an intact sample (a) pore water pressure against cycle number and (b)
755 shear stress against normal effective stress.

756
757 Figure 13. Dynamic shear stage of testing at a frequency of 2 Hz for 10 cycles of 1
758 minute duration (a) pore water pressure against cycle number and (b) shear stress
759 against normal effective stress.

760
761 Figure 14. Dynamic shear stage of testing at a frequency of 2 Hz for a duration of 10
762 minutes on a remoulded sample (a) pore water pressure against cycle number and (b)
763 shear stress against normal effective stress.

764
765 Figure 15. Dynamic shear stage of samples undergoing dynamic liquefaction (a) shear
766 stress against normal effective stress (c) Pore water pressure against change in sample
767 volume.

768
769 Figure 16. Change in sample height of intact sample DYN6 and remoulded sample
770 DYN7 during the dynamic shear stage of testing at a frequency of 2hz for a duration
771 of 10 minutes (1200 cycles).

772
773 Figure 17. Dynamic shear stage of samples not undergoing dynamic liquefaction (a)
774 shear stress against normal effective stress (c) Pore water pressure against change in
775 sample volume.

776

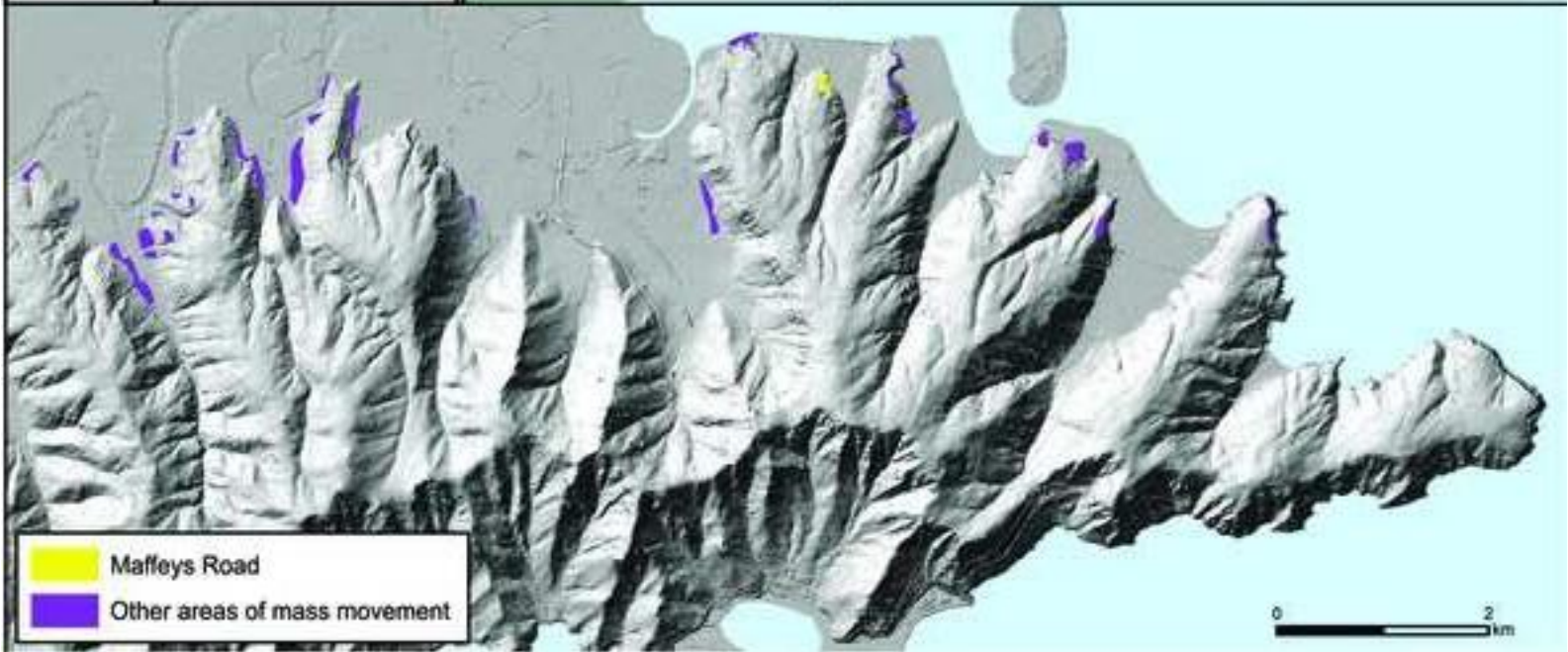
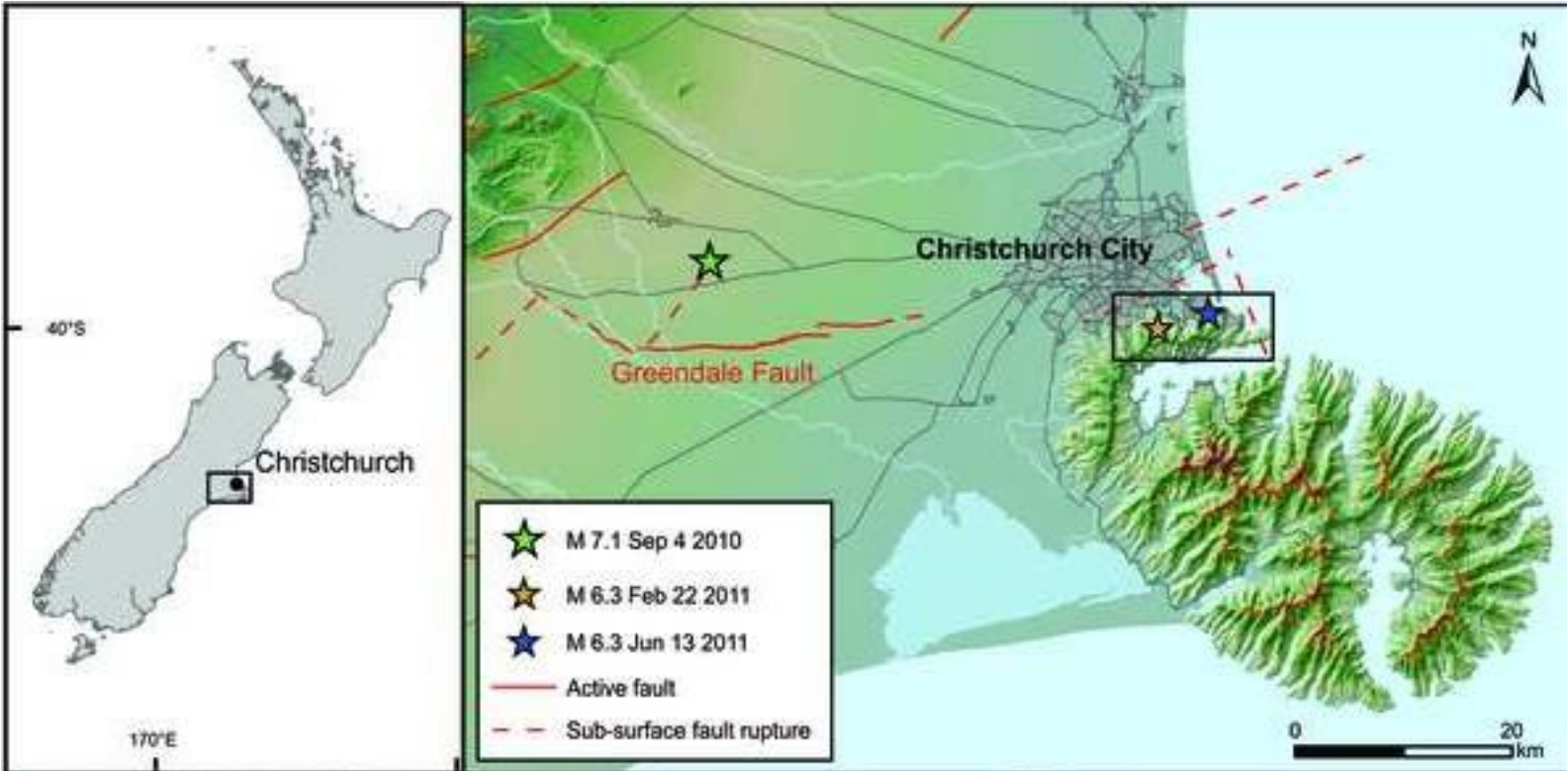
777 Figure 18. Dynamic shear stage of remoulded sample DYN7 and post dynamic
778 liquefaction repeat cycles of sample DYN5 (a) Pore water pressure against vertical
779 strain (b) Shear stress against normal effective stress.

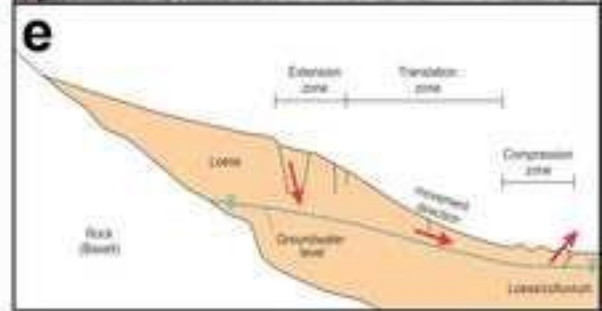
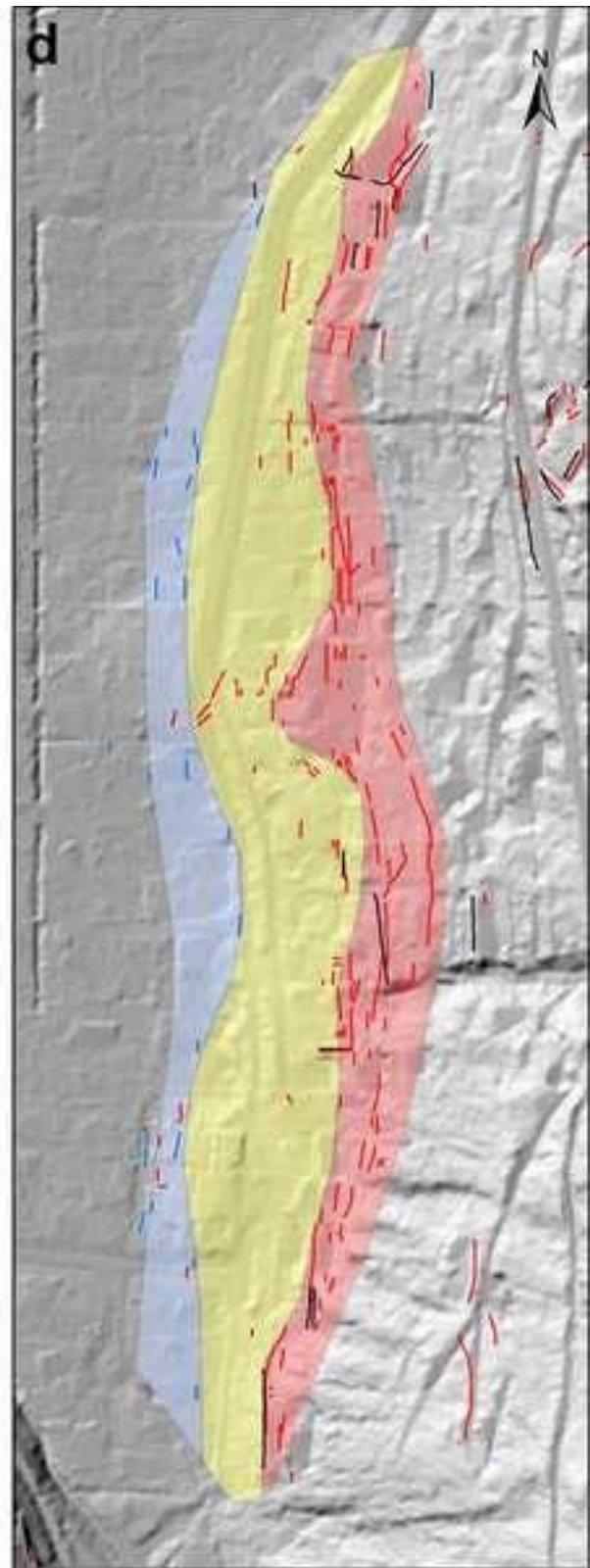
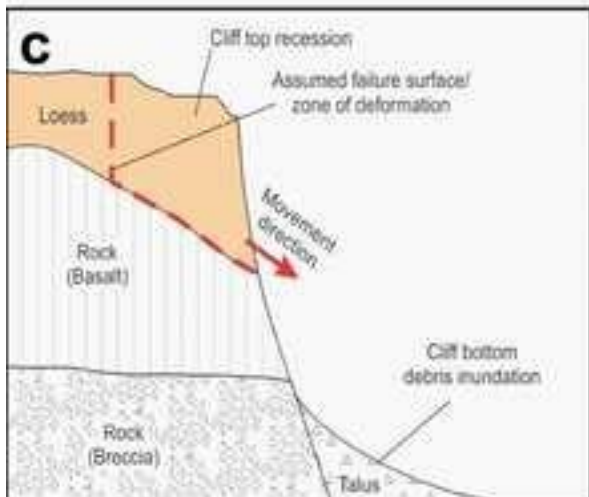
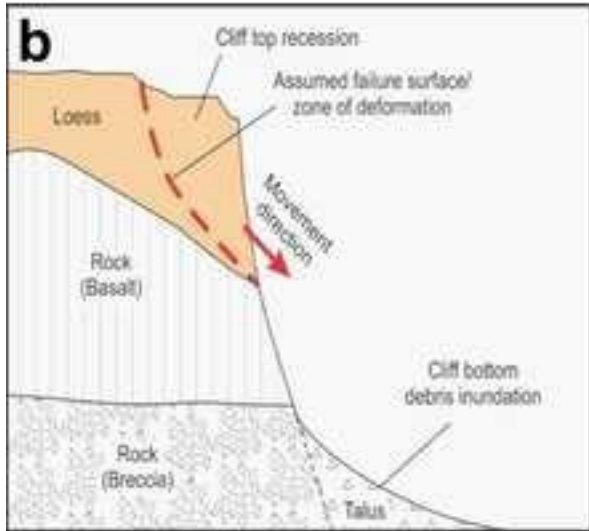
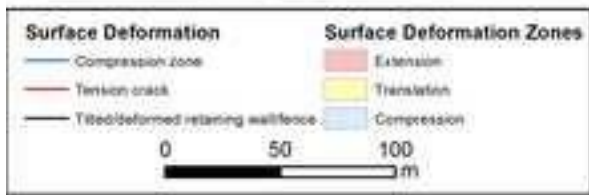
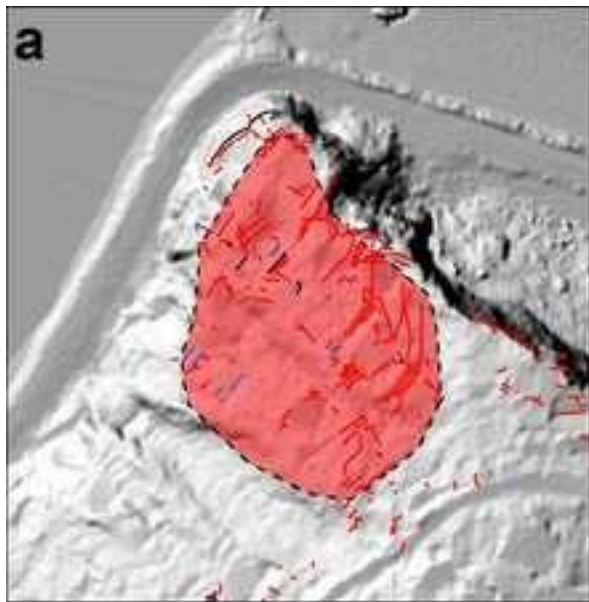
780

781 TABLES

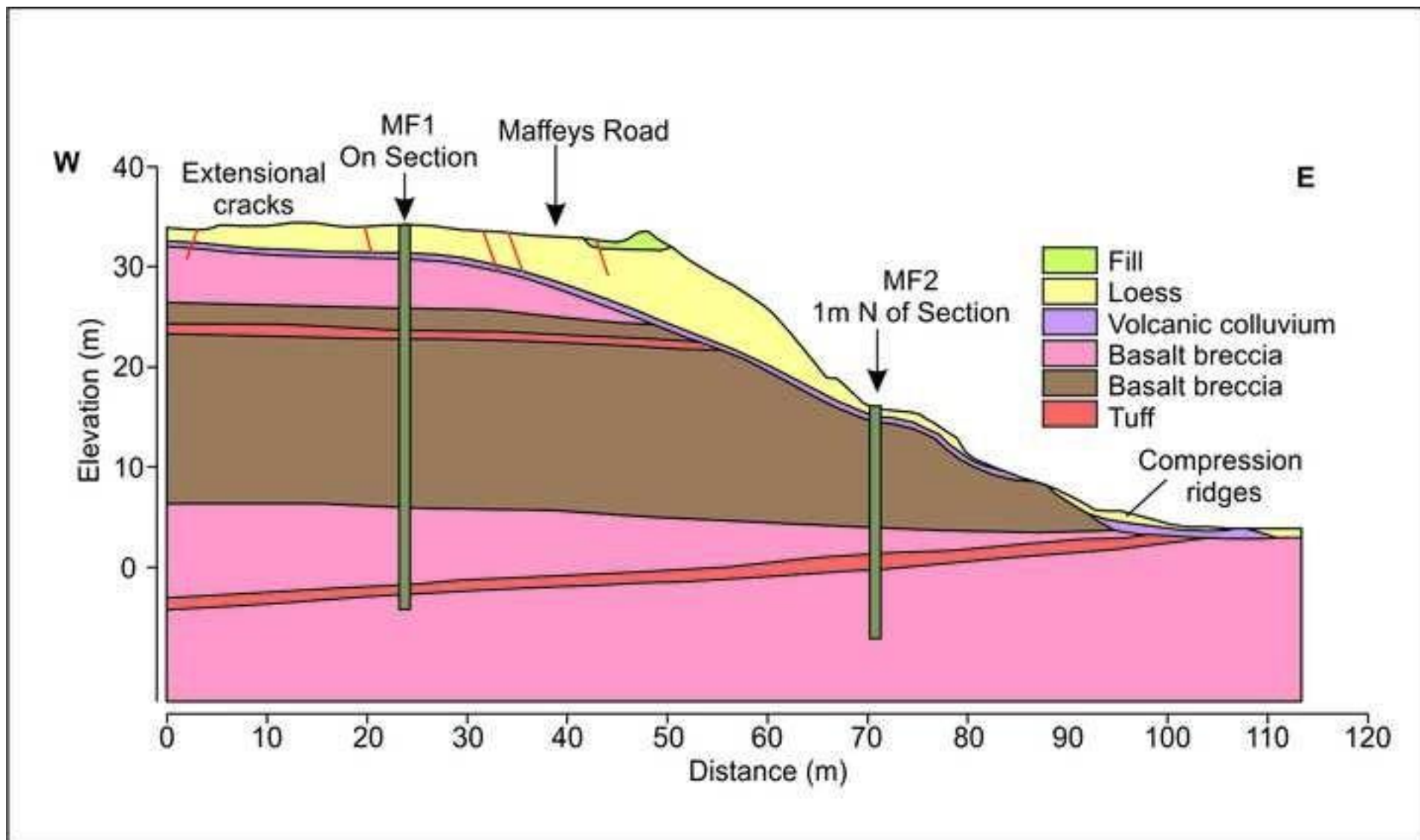
782 Table 1. Loess physical properties

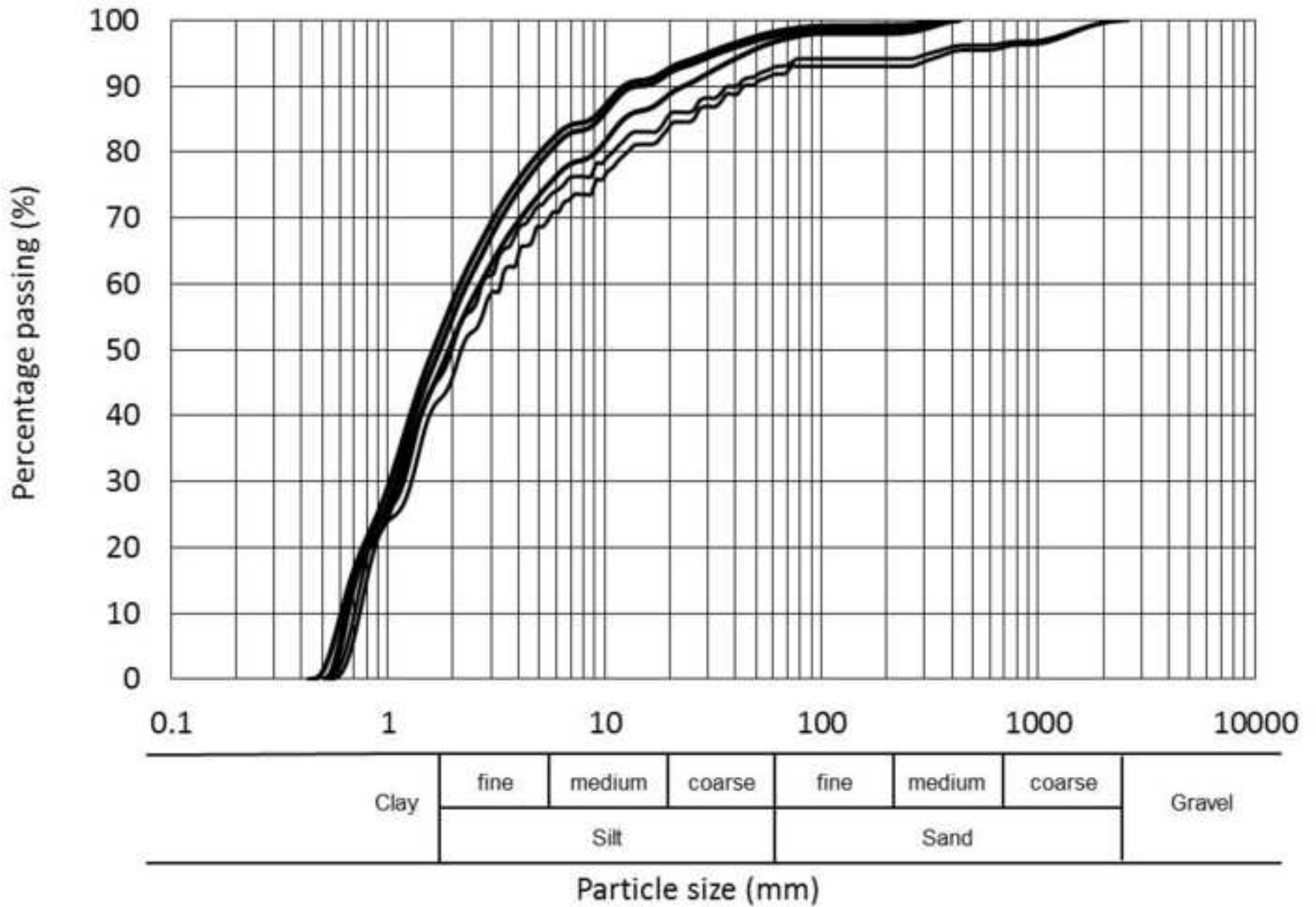
783 Table 2. Summary of laboratory tests.

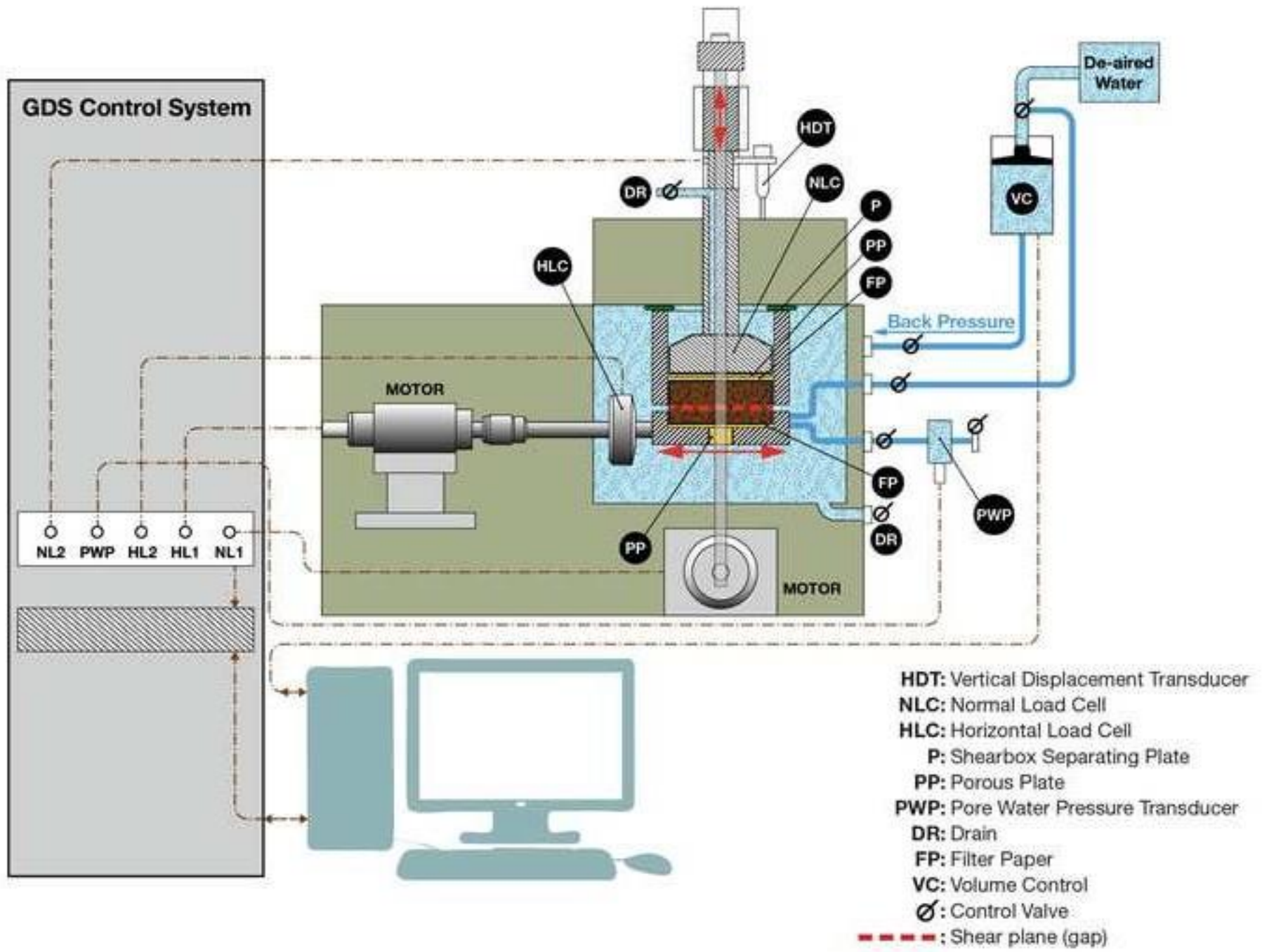


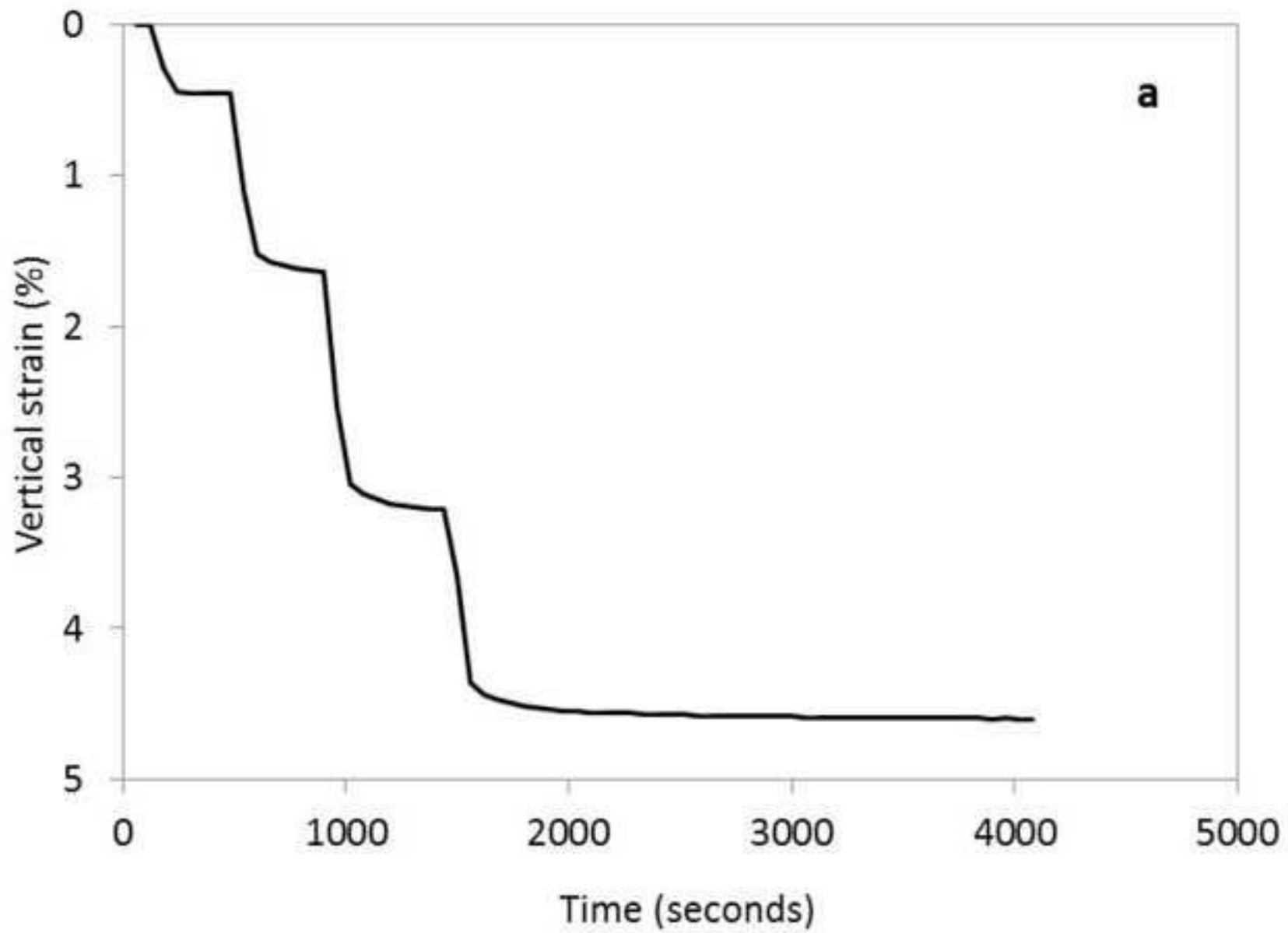




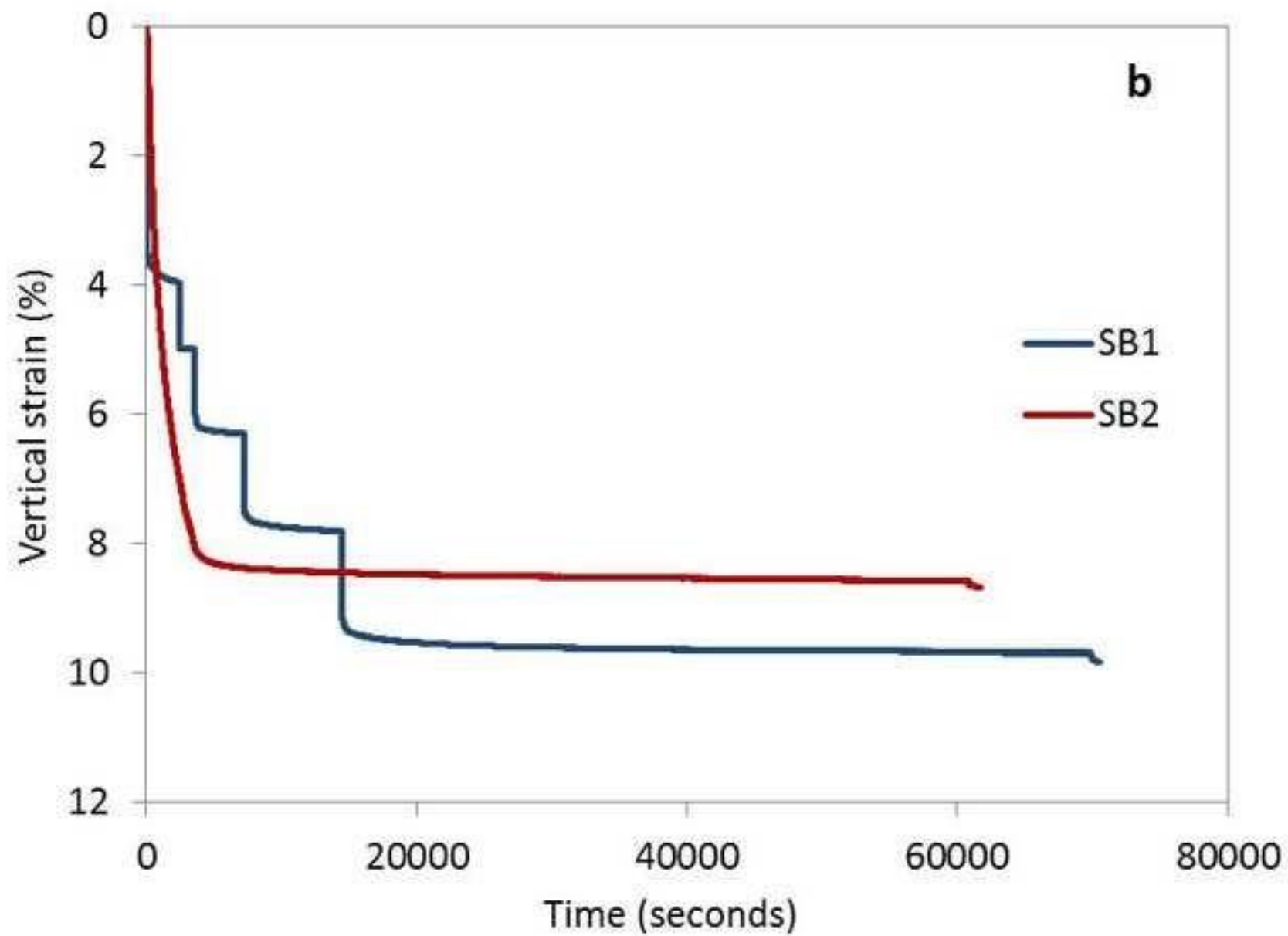


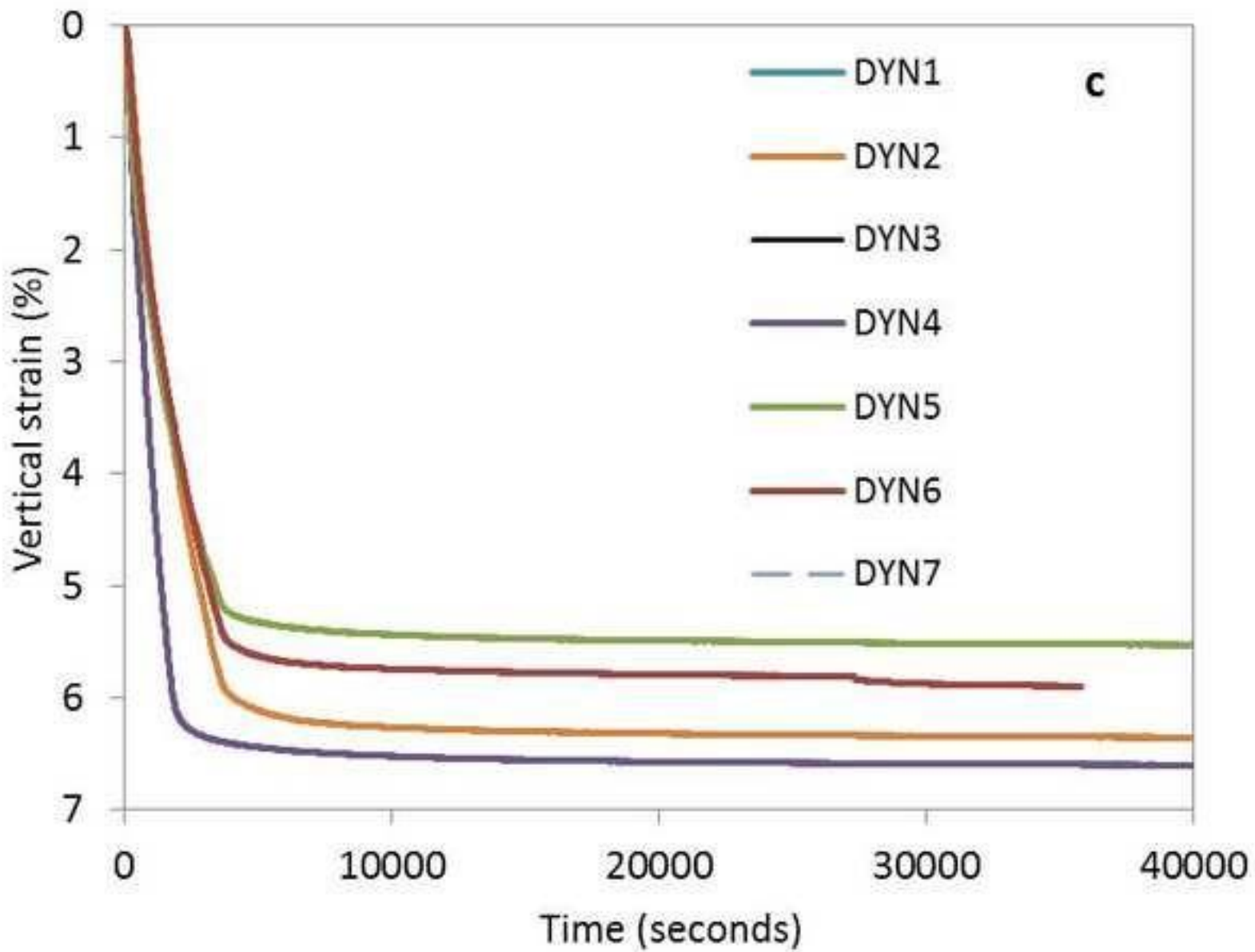


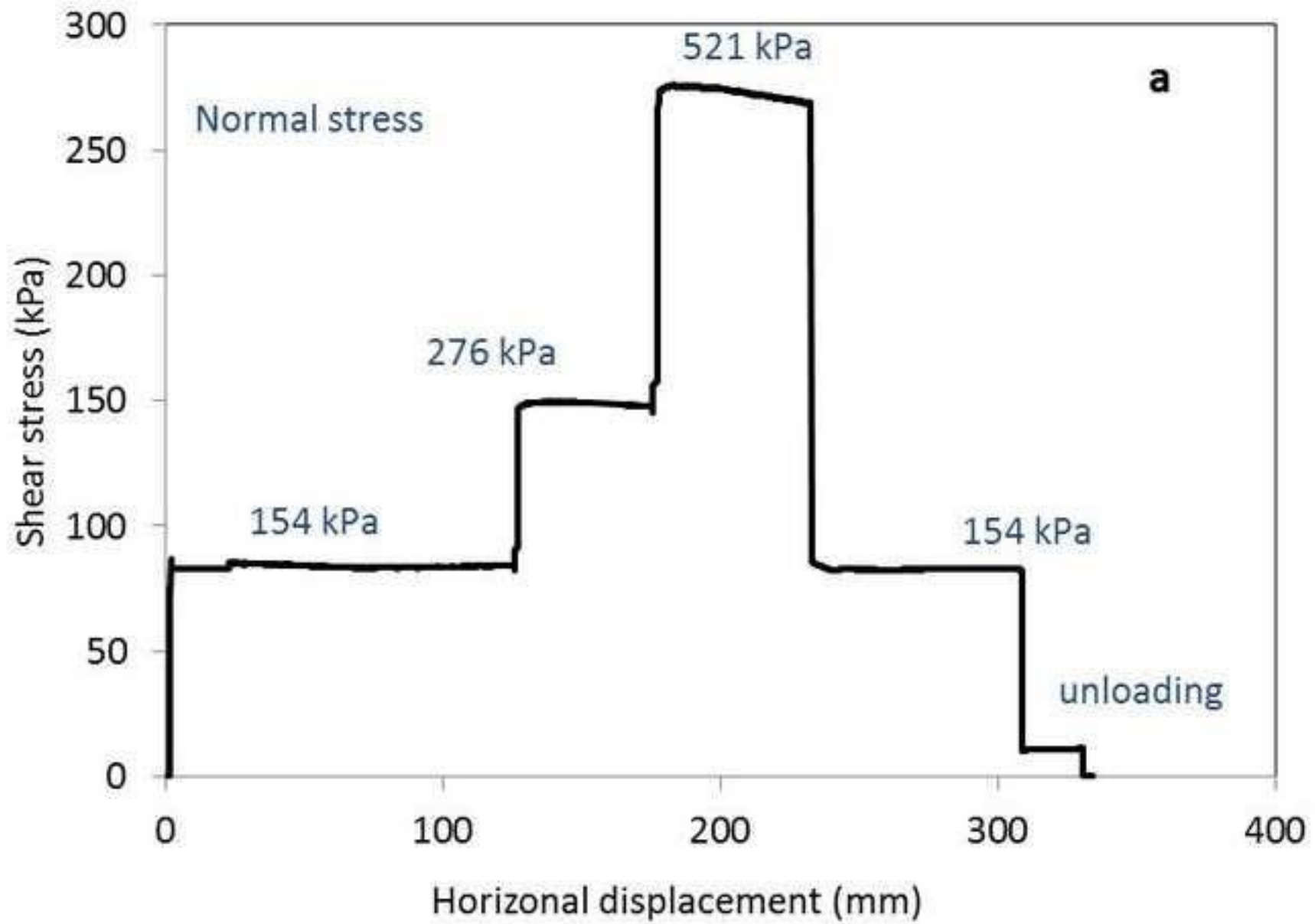


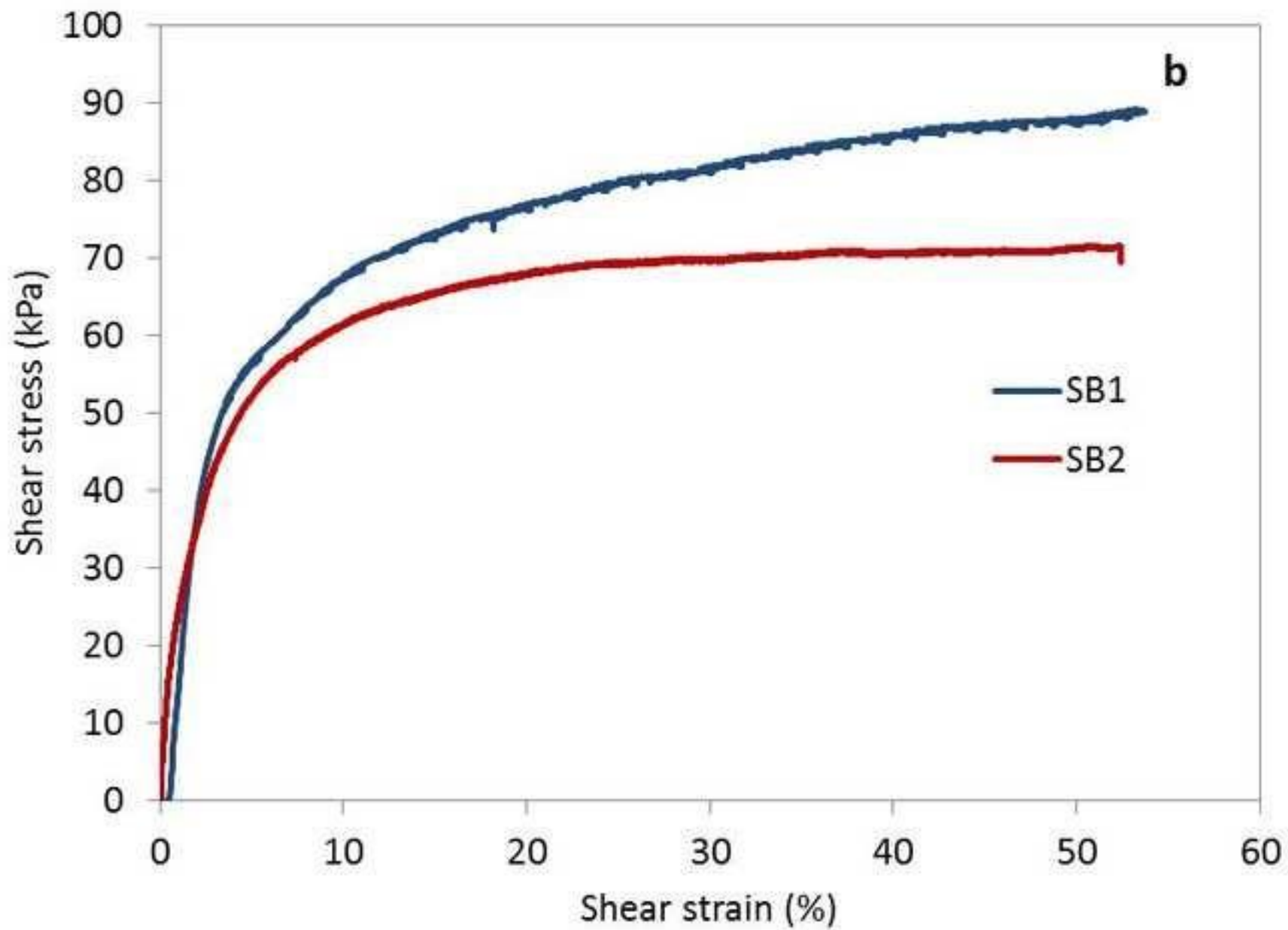


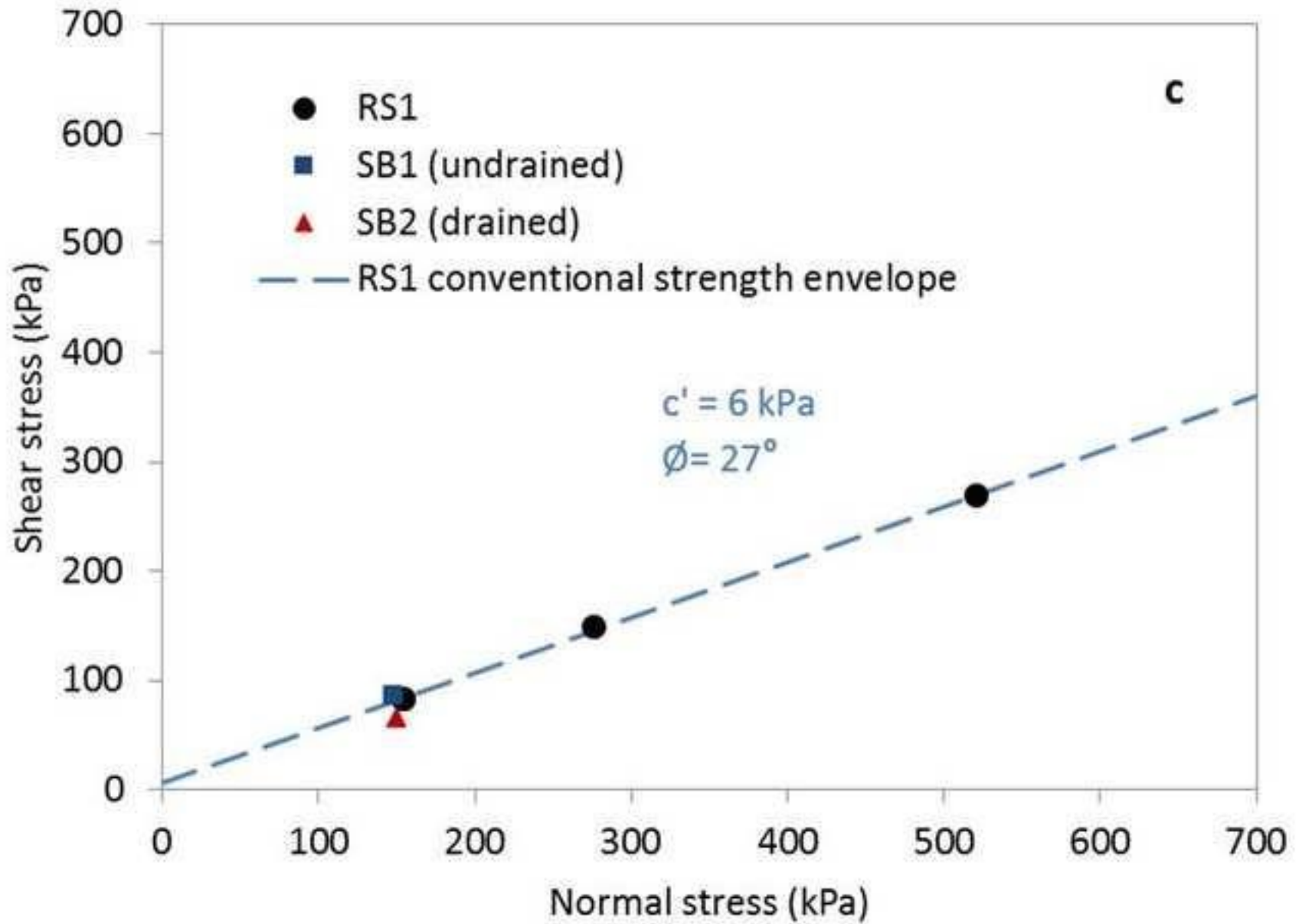
a

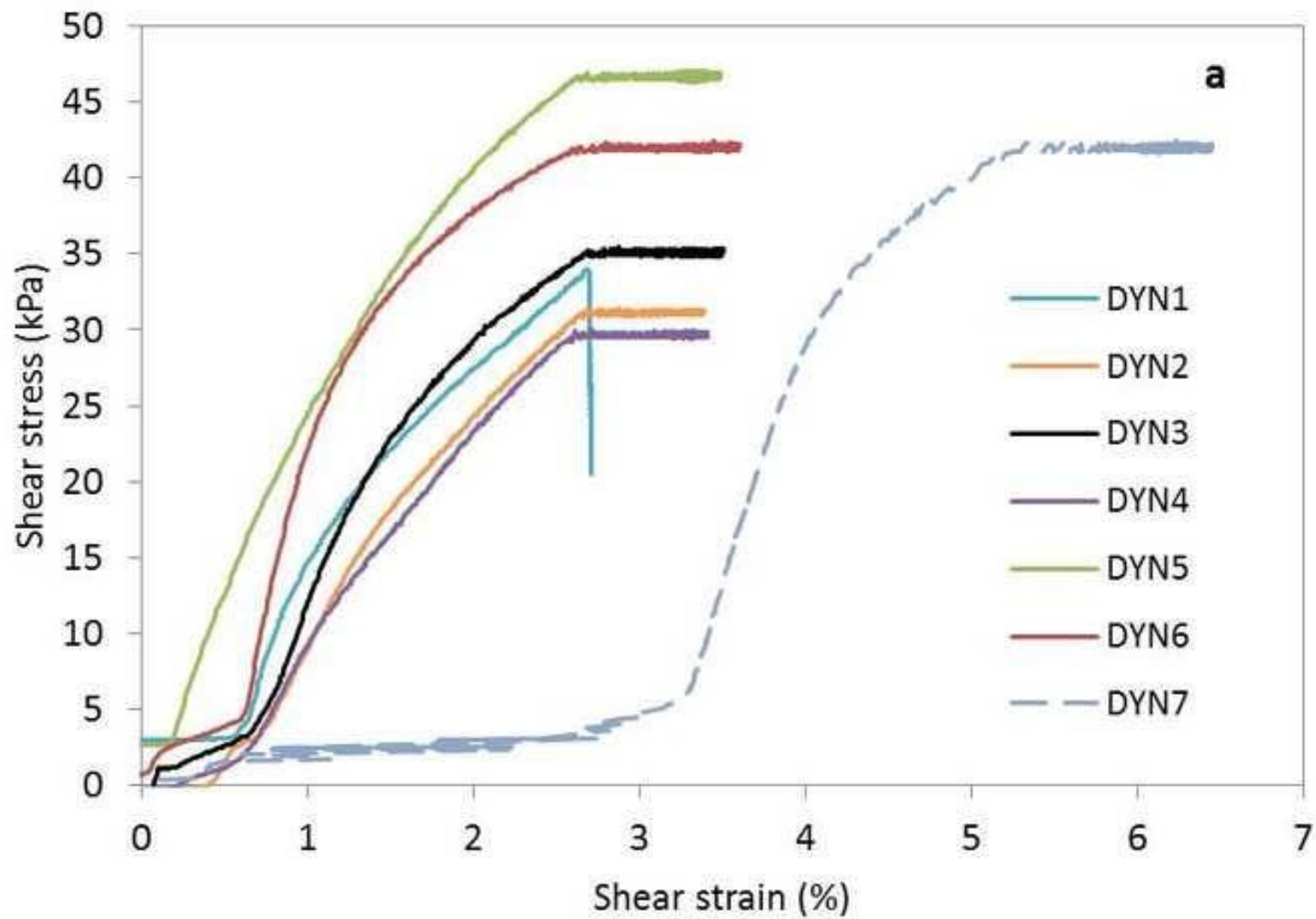


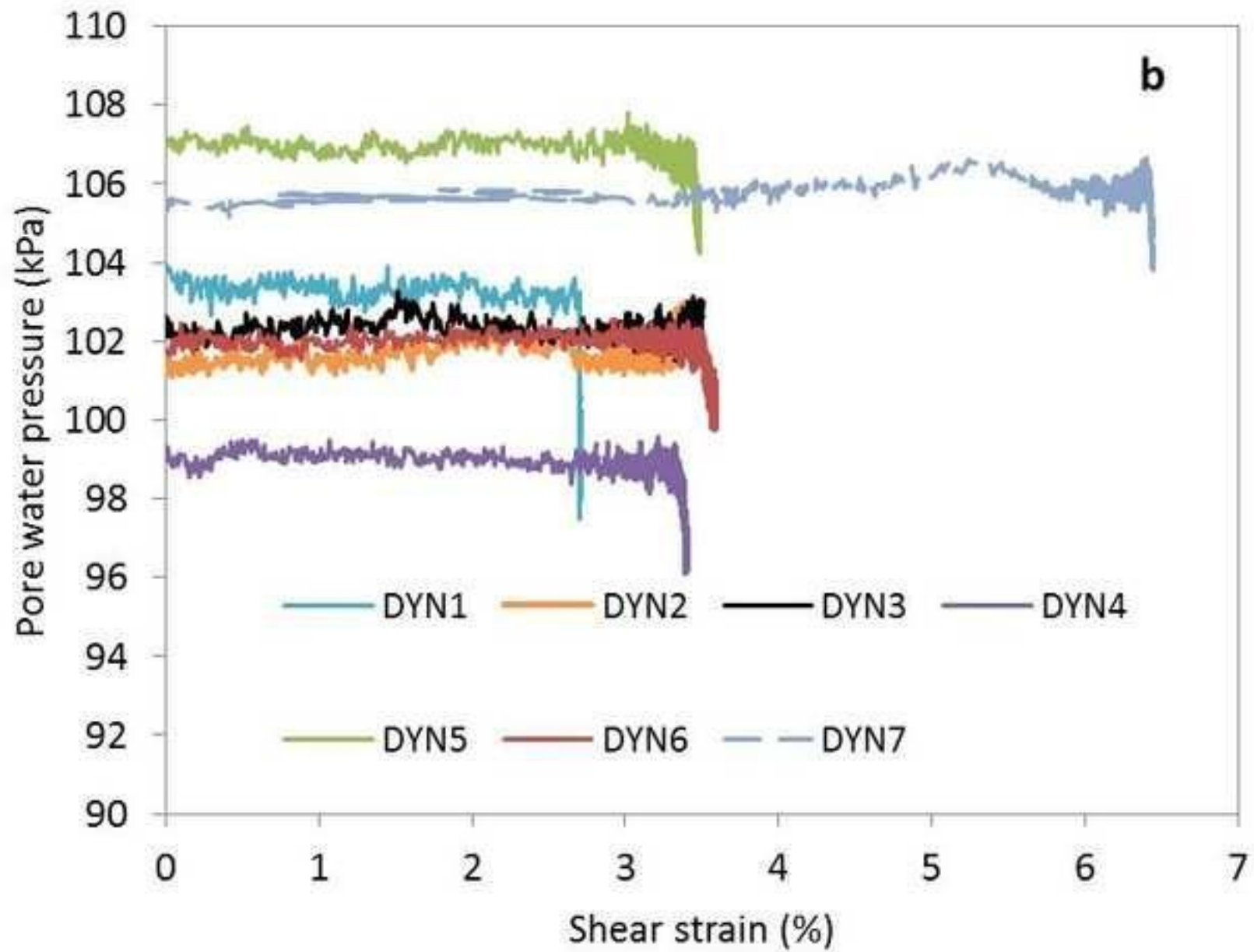


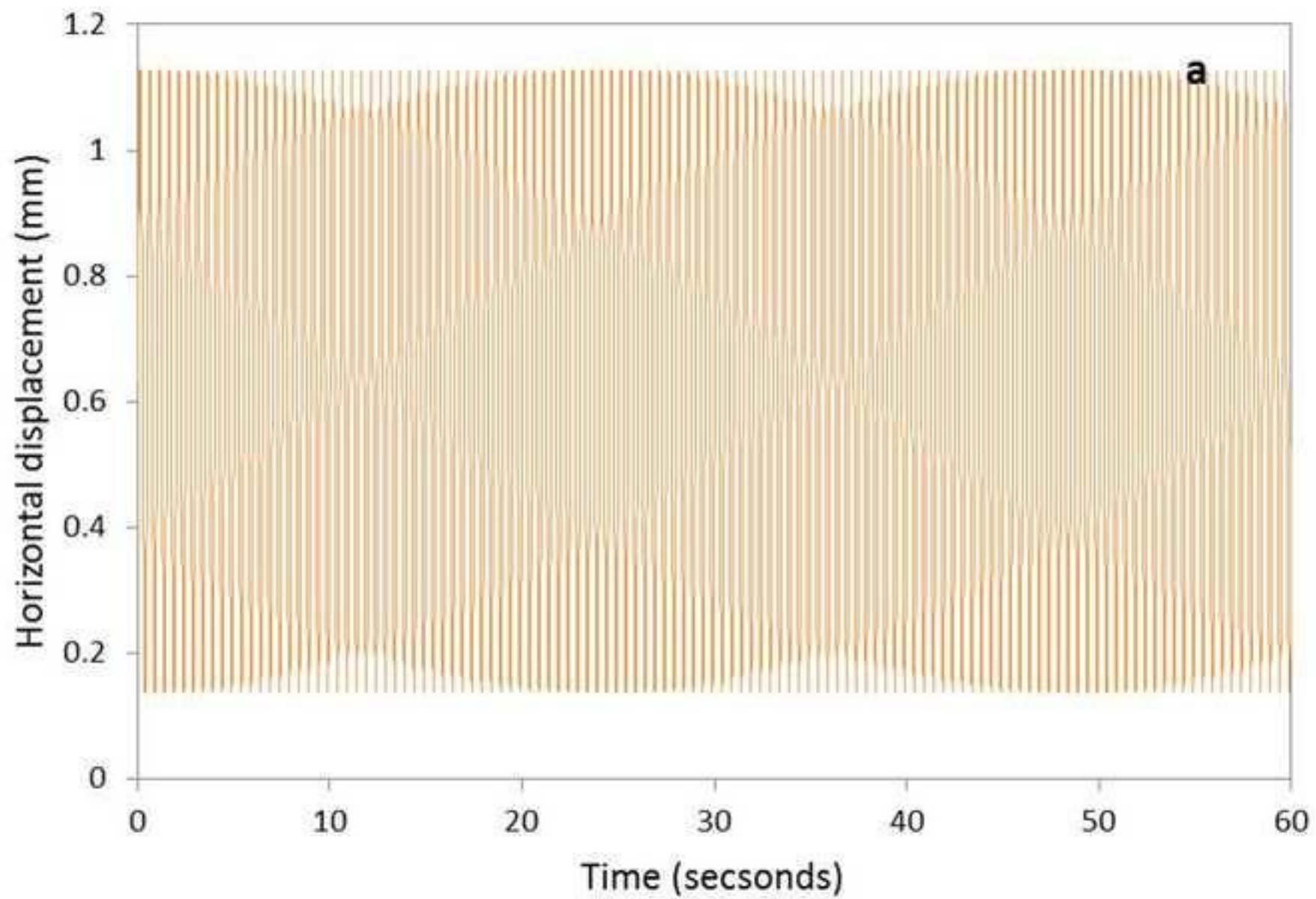


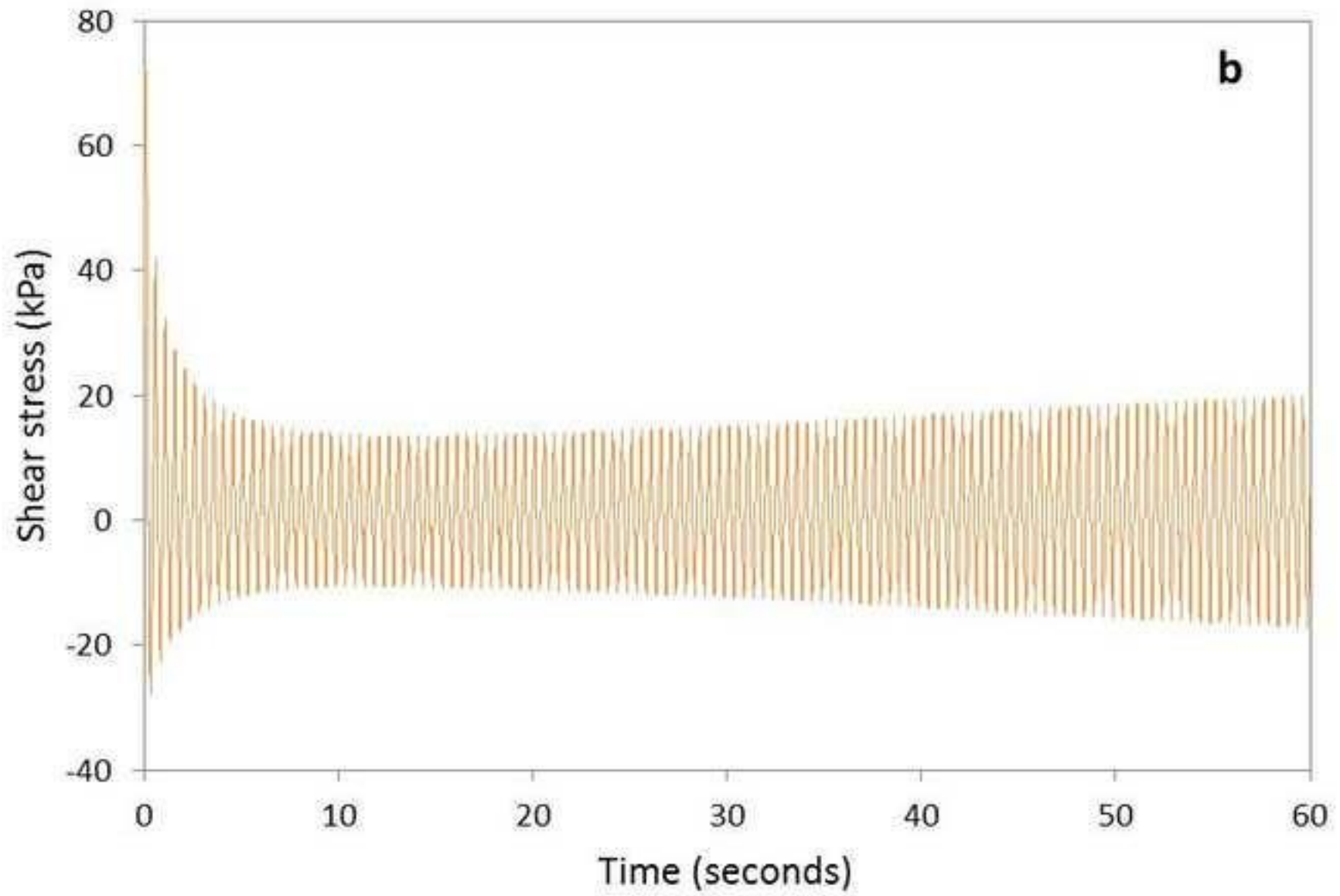




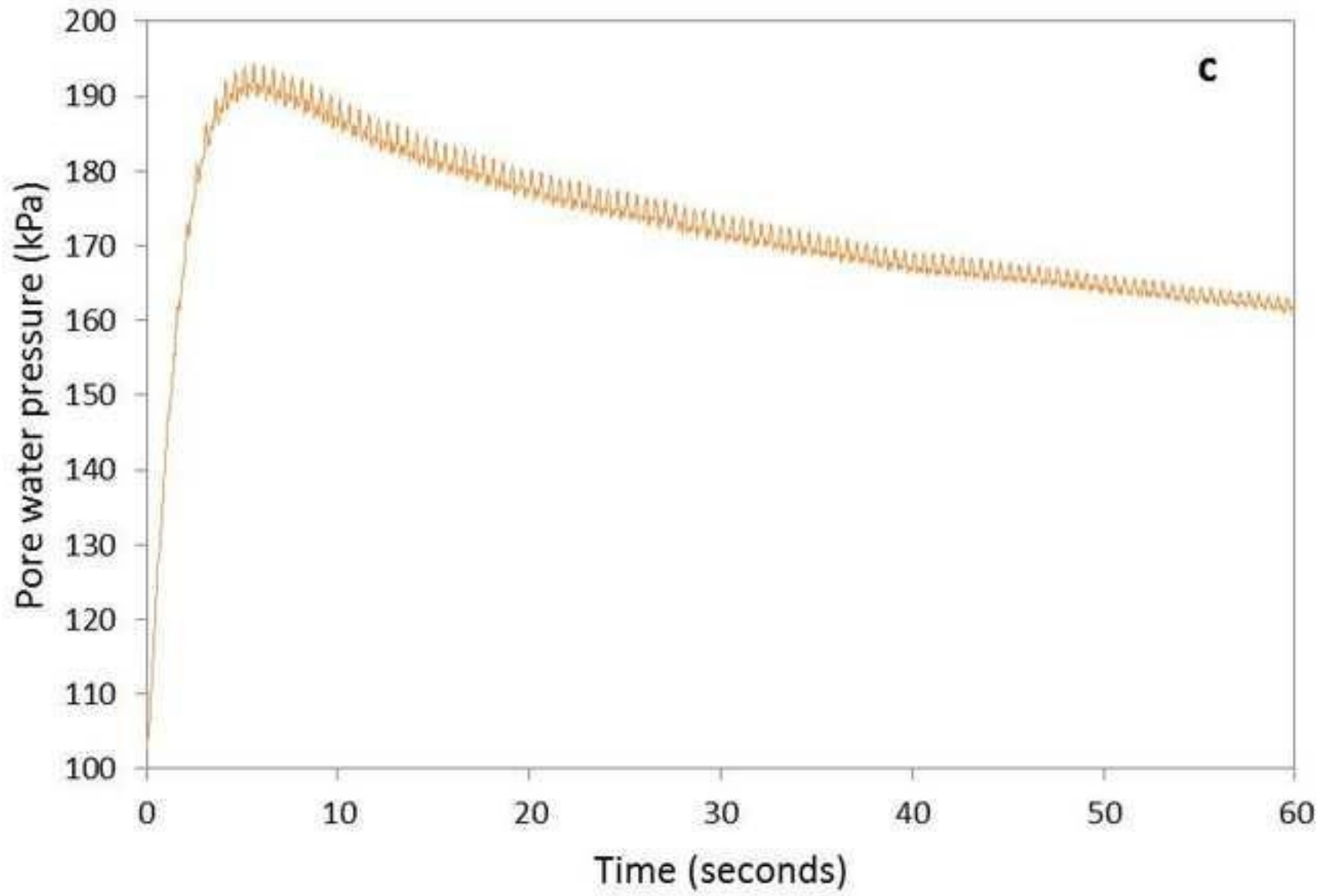


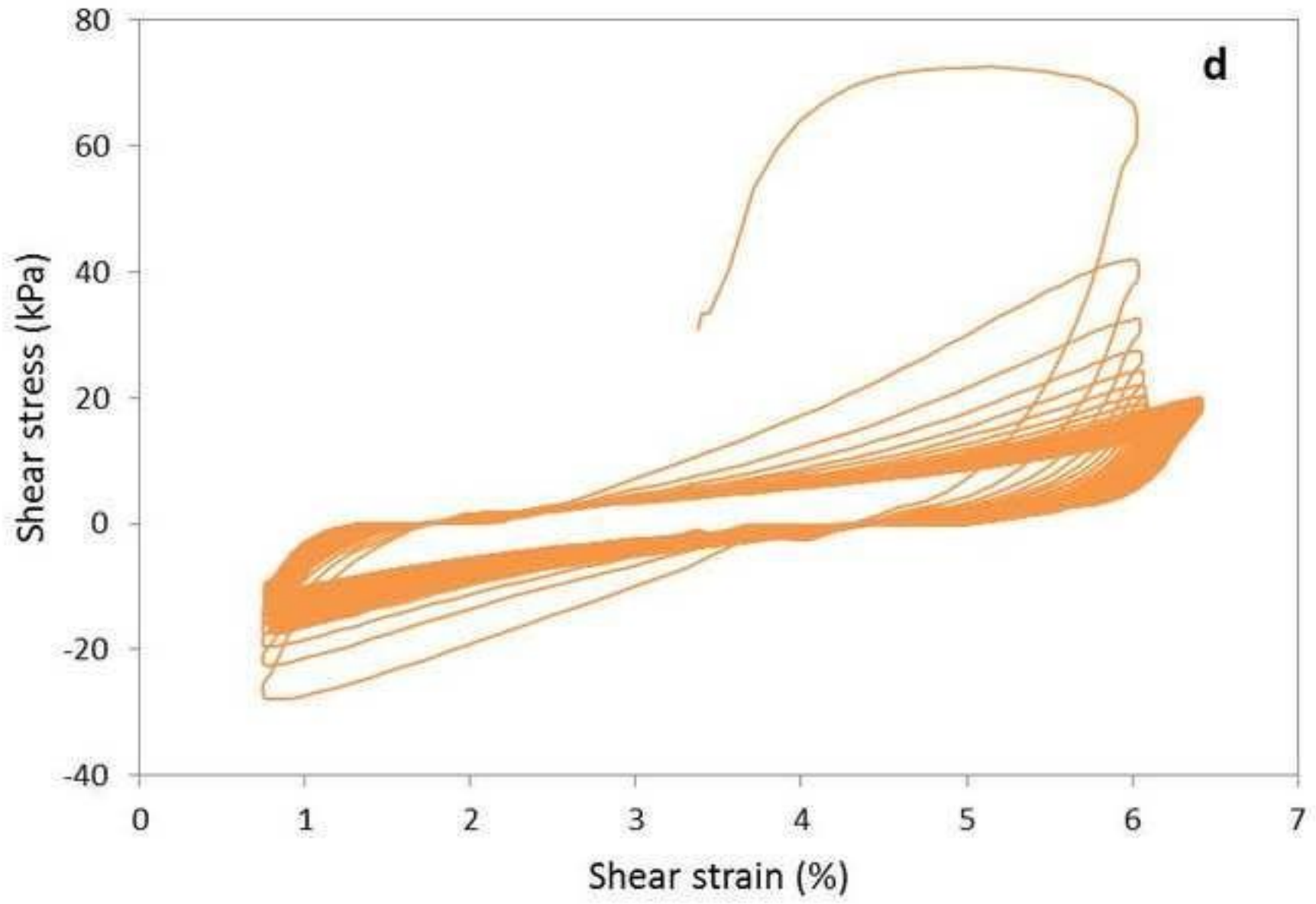


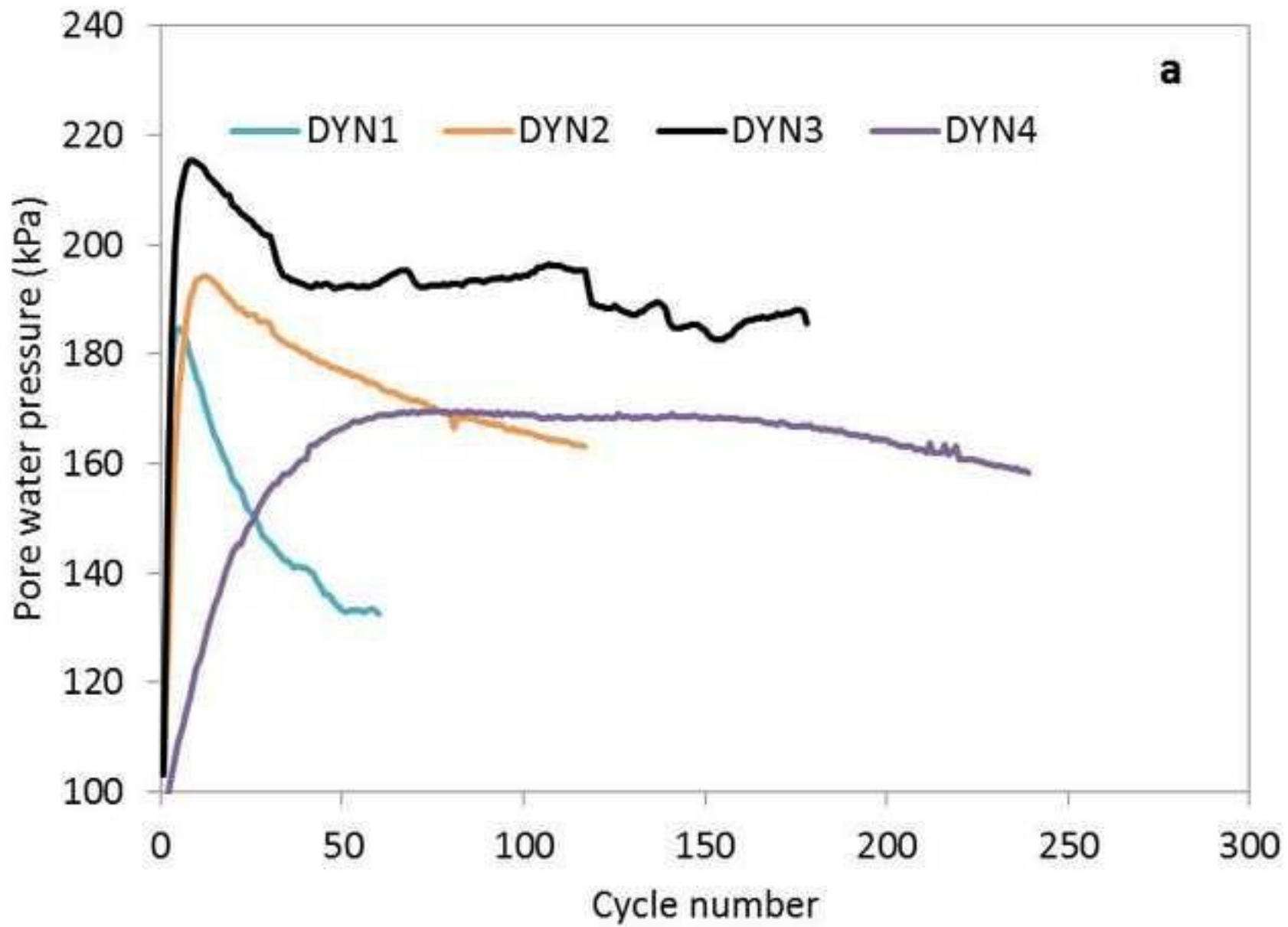


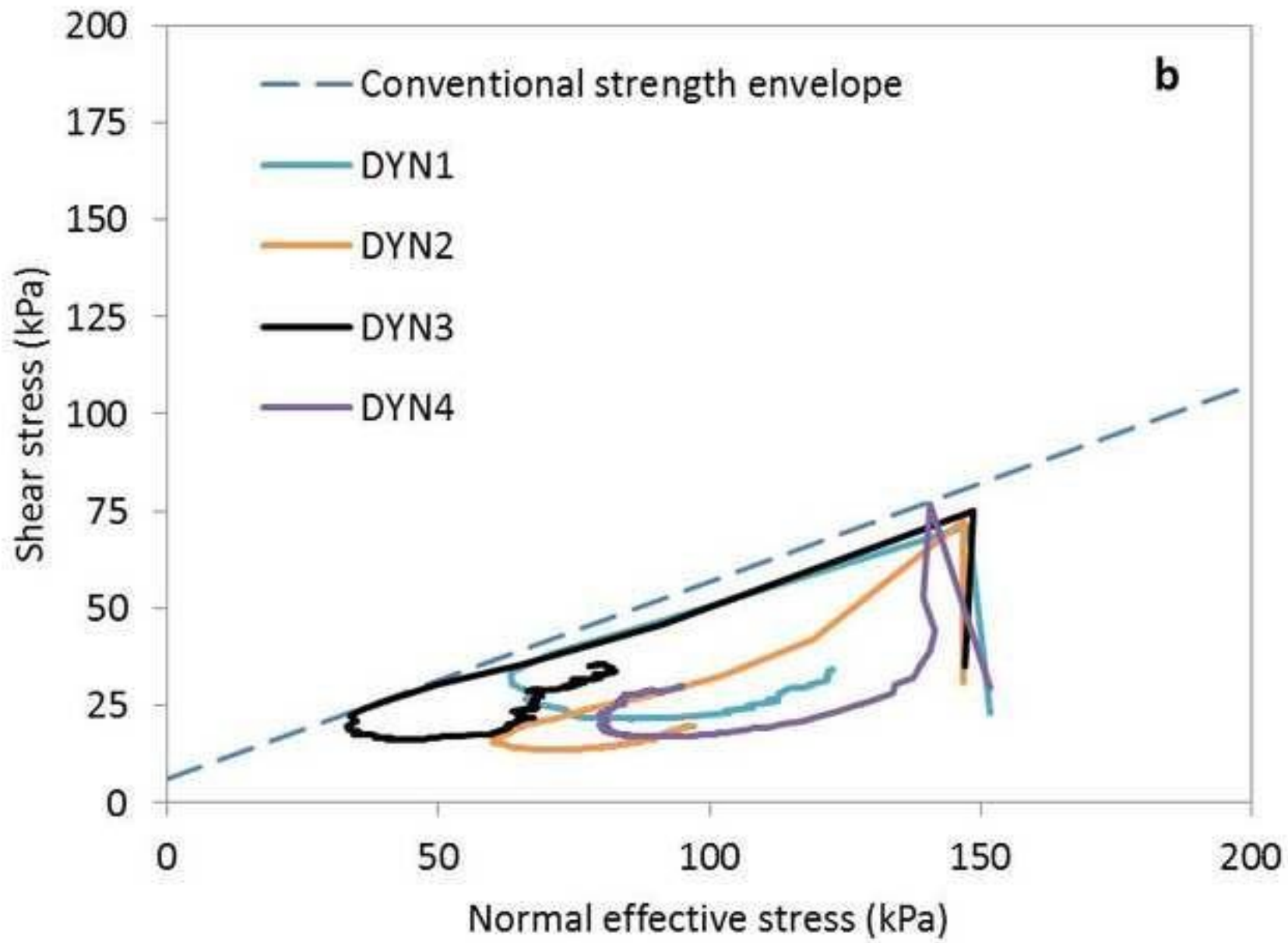


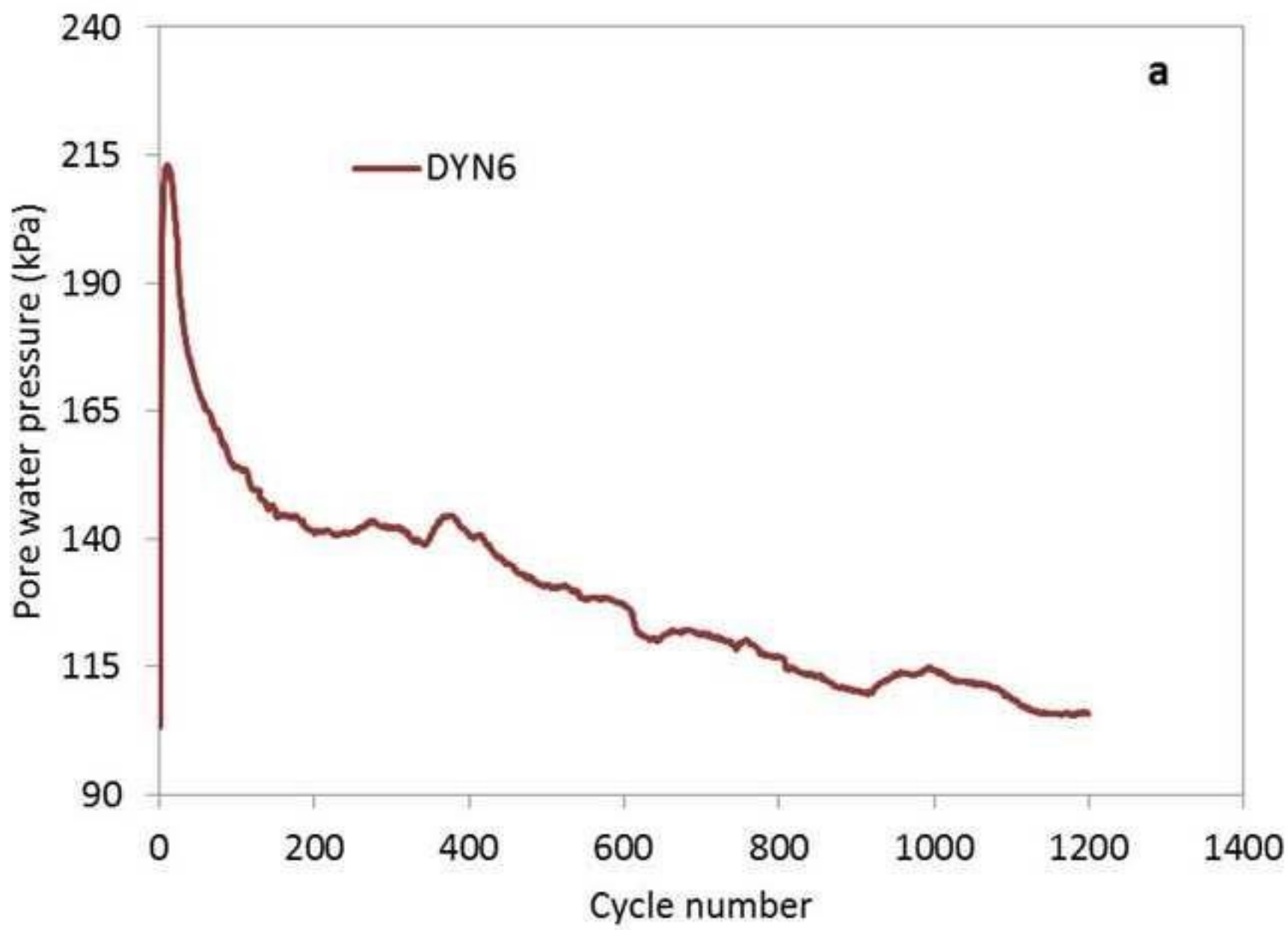
b



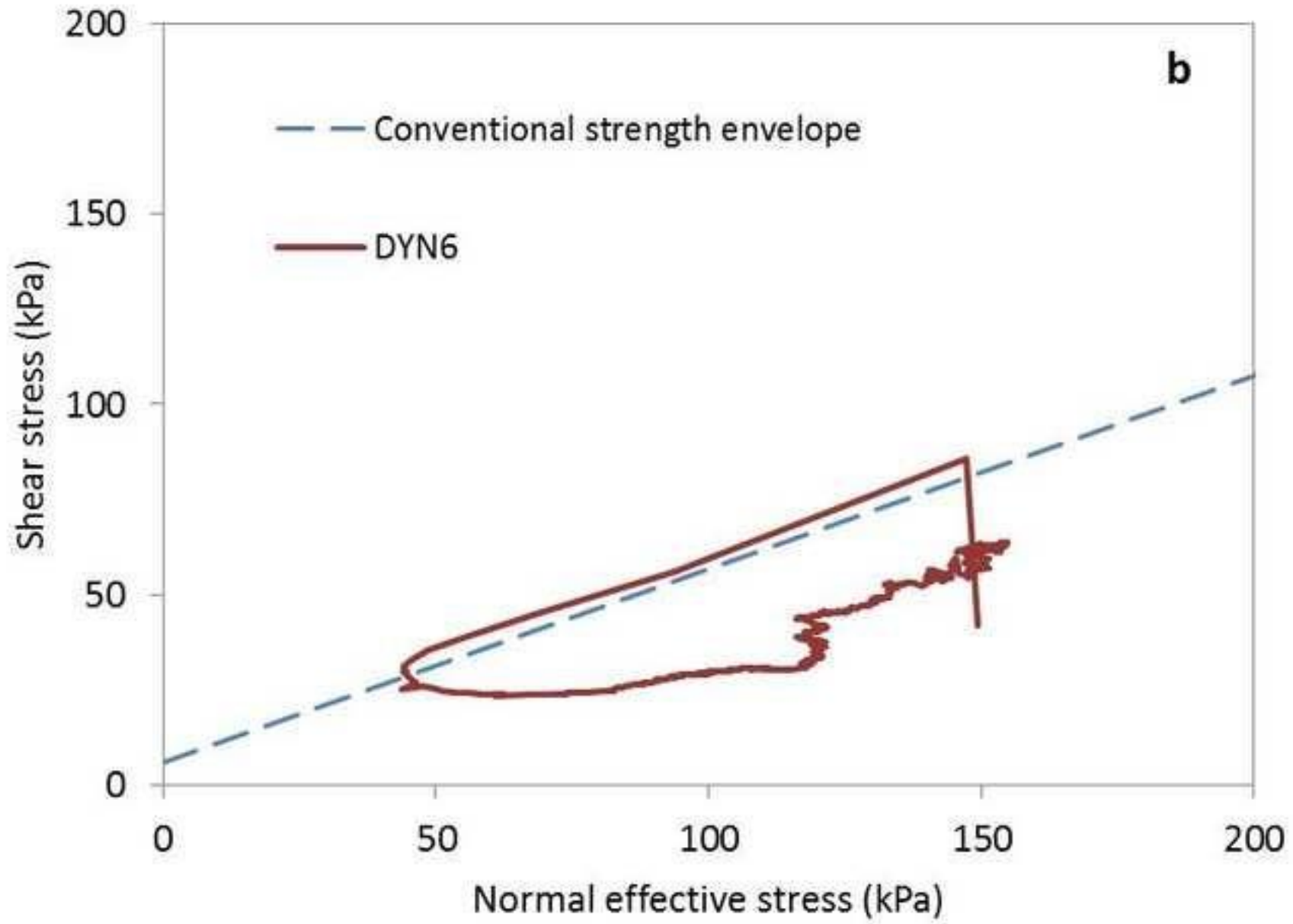


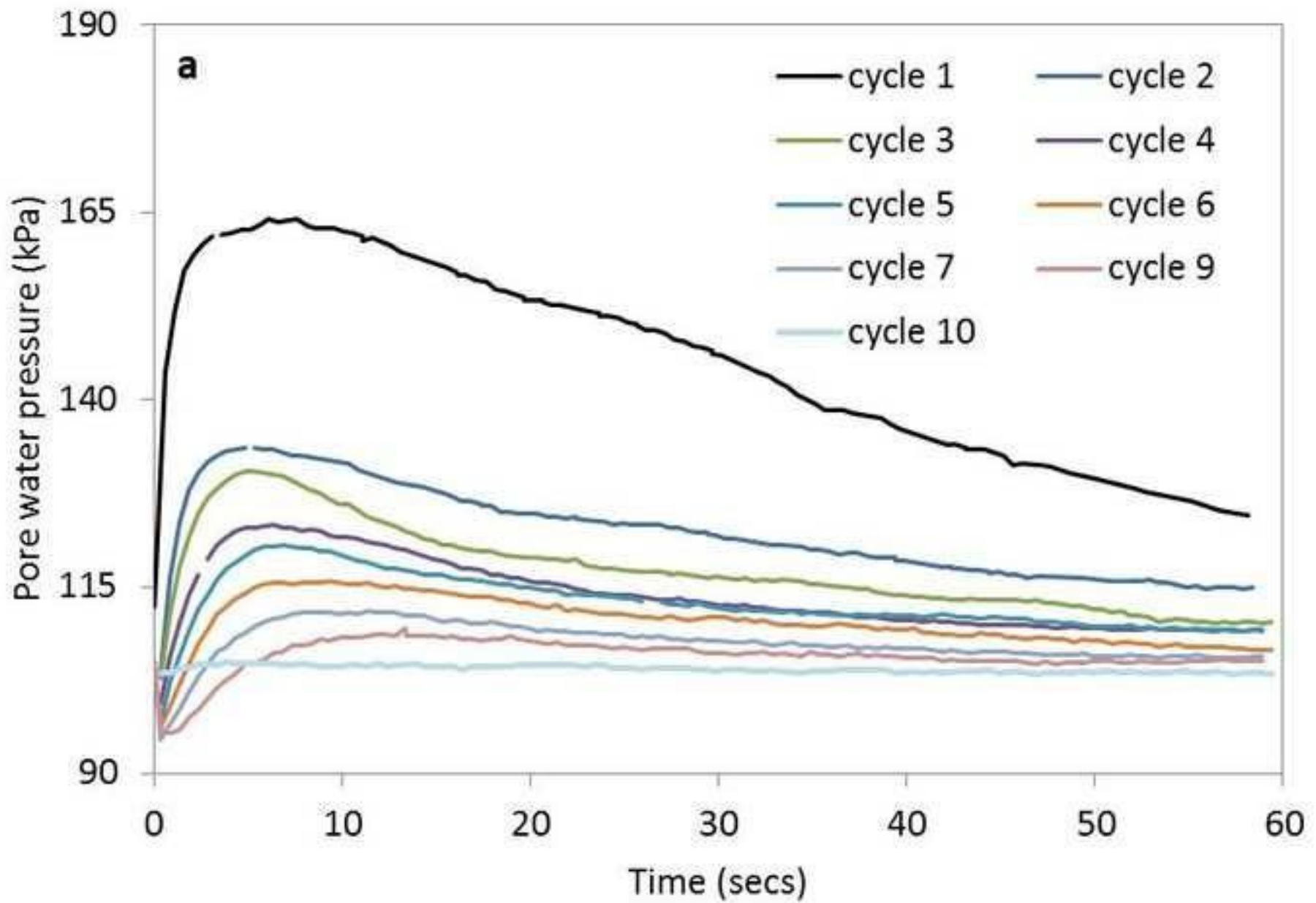


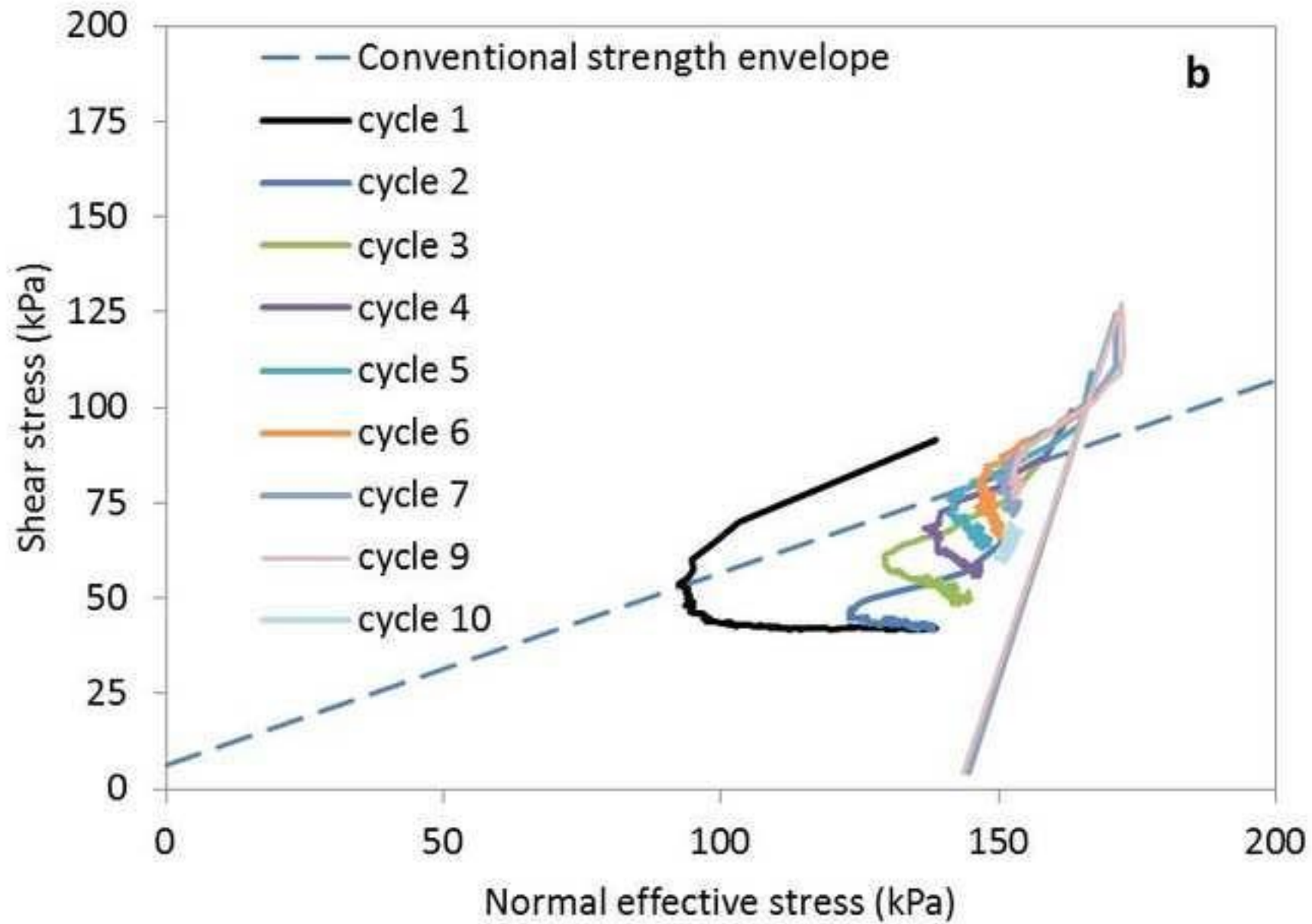


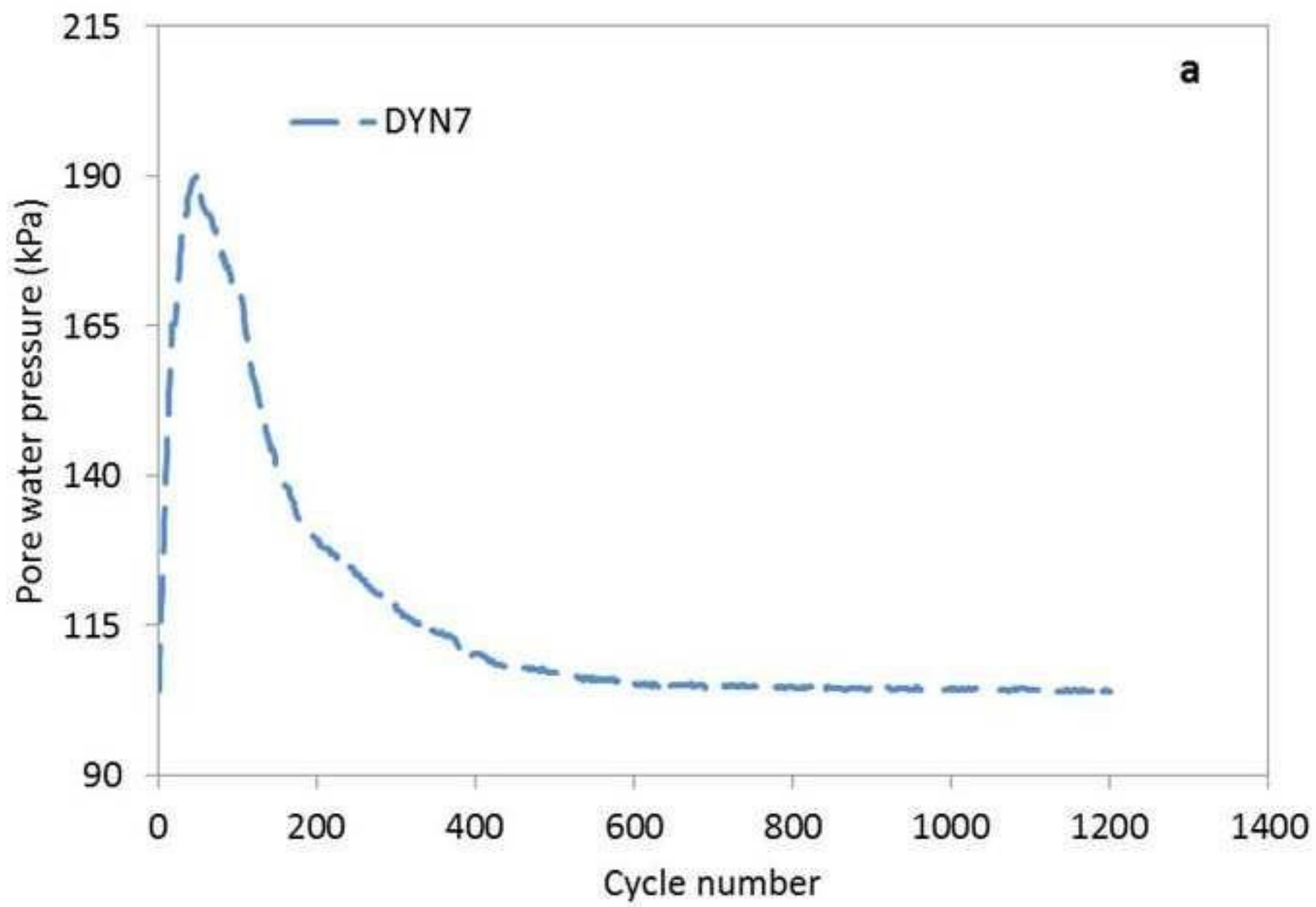


b

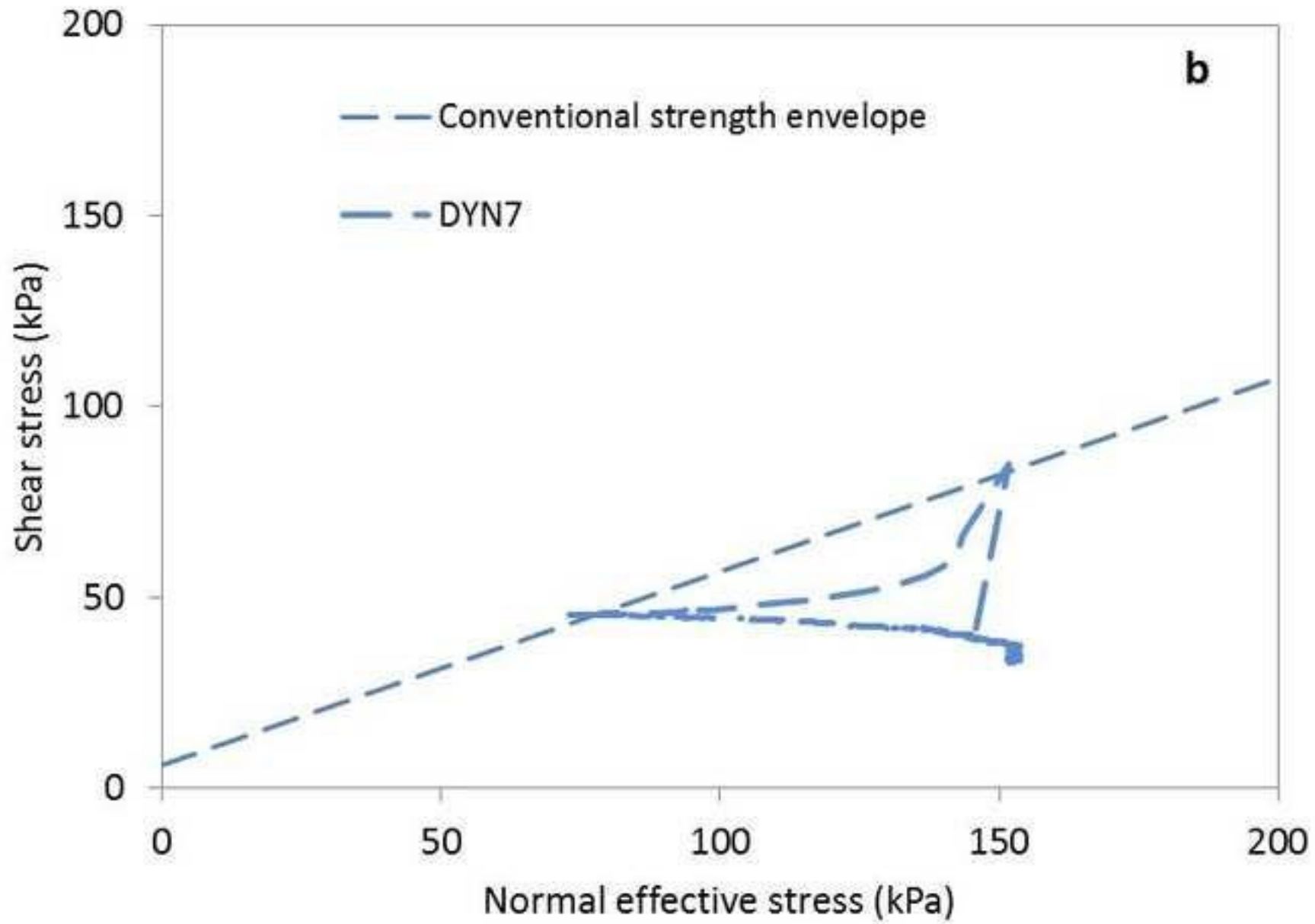


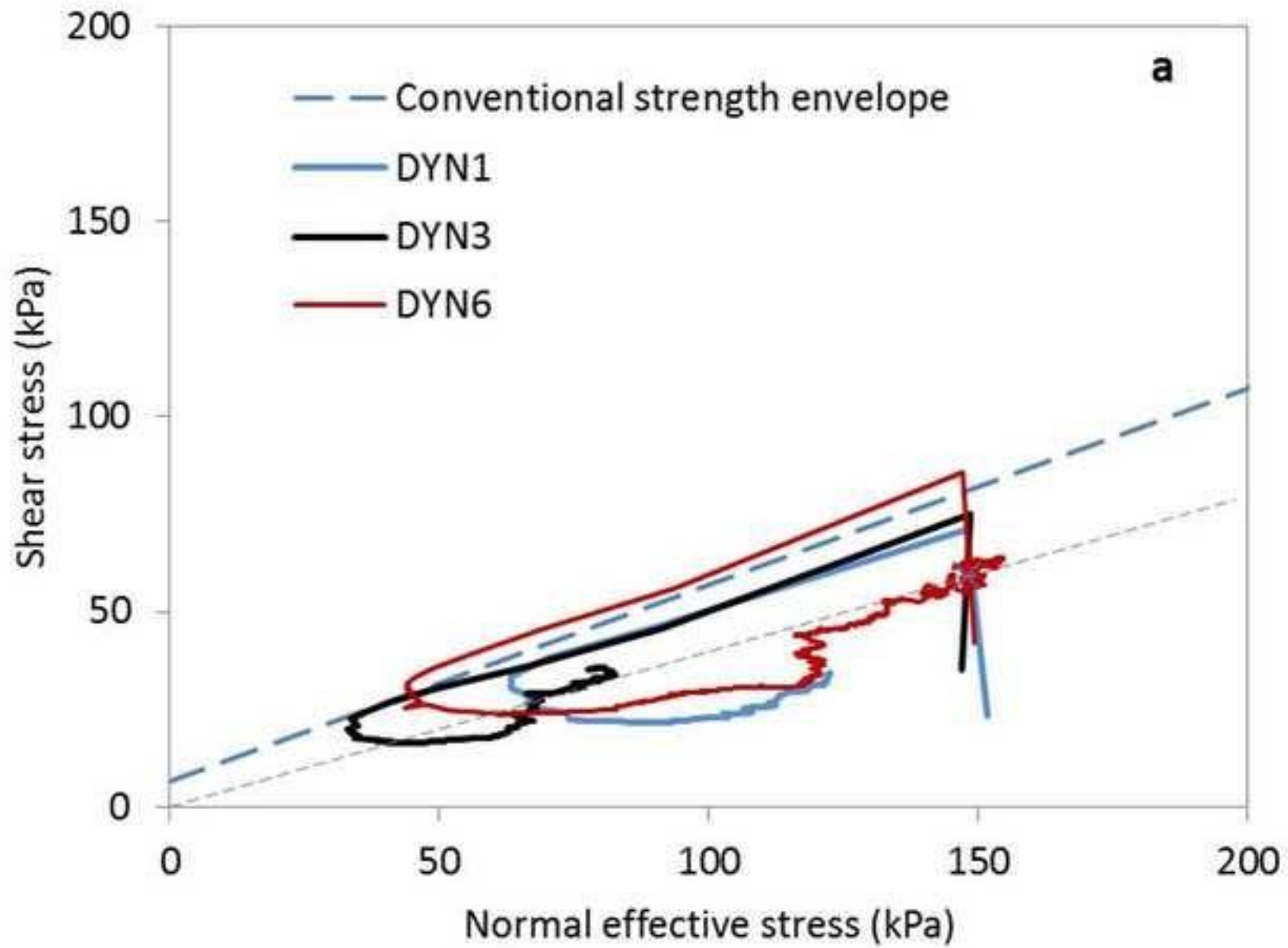


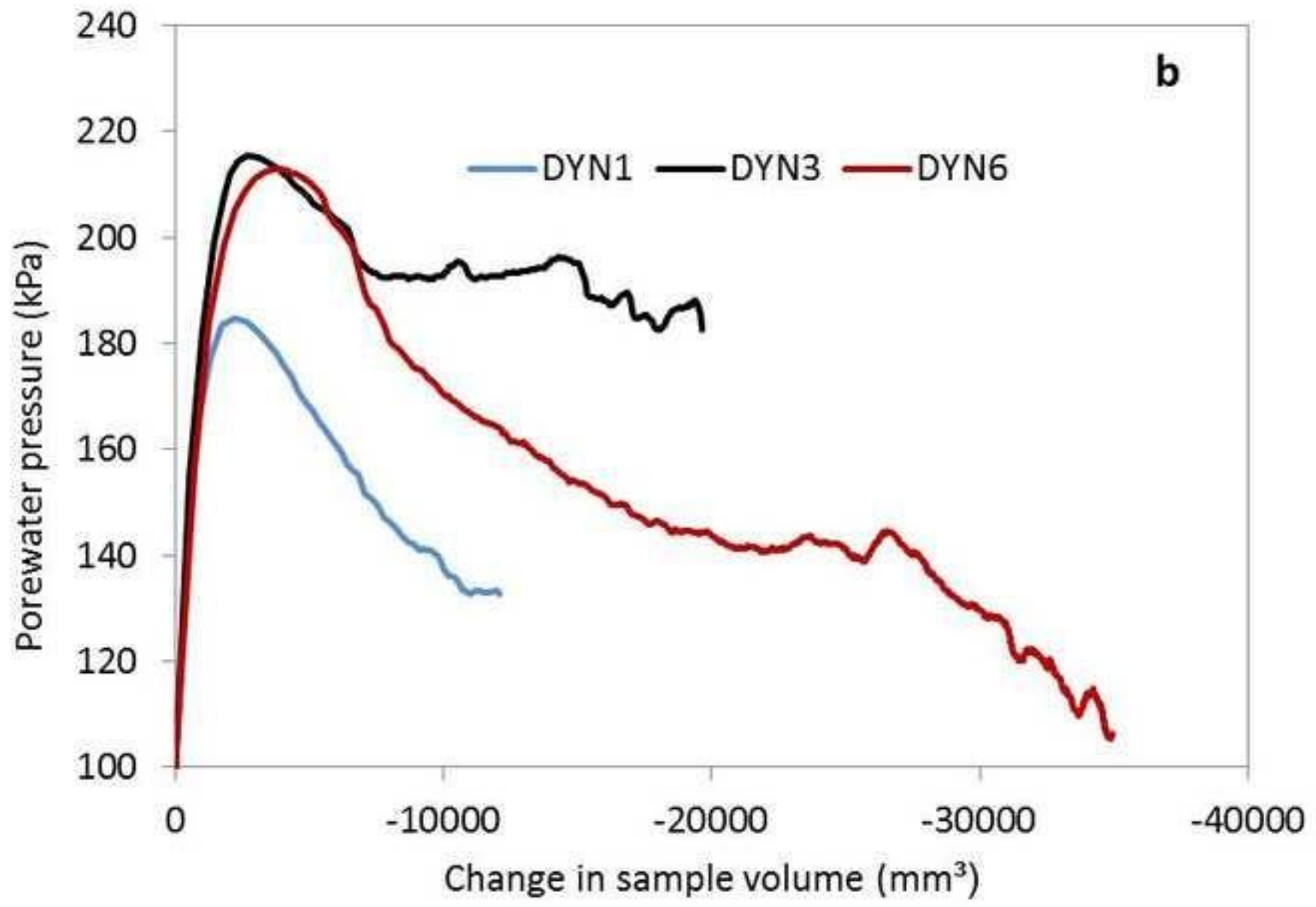


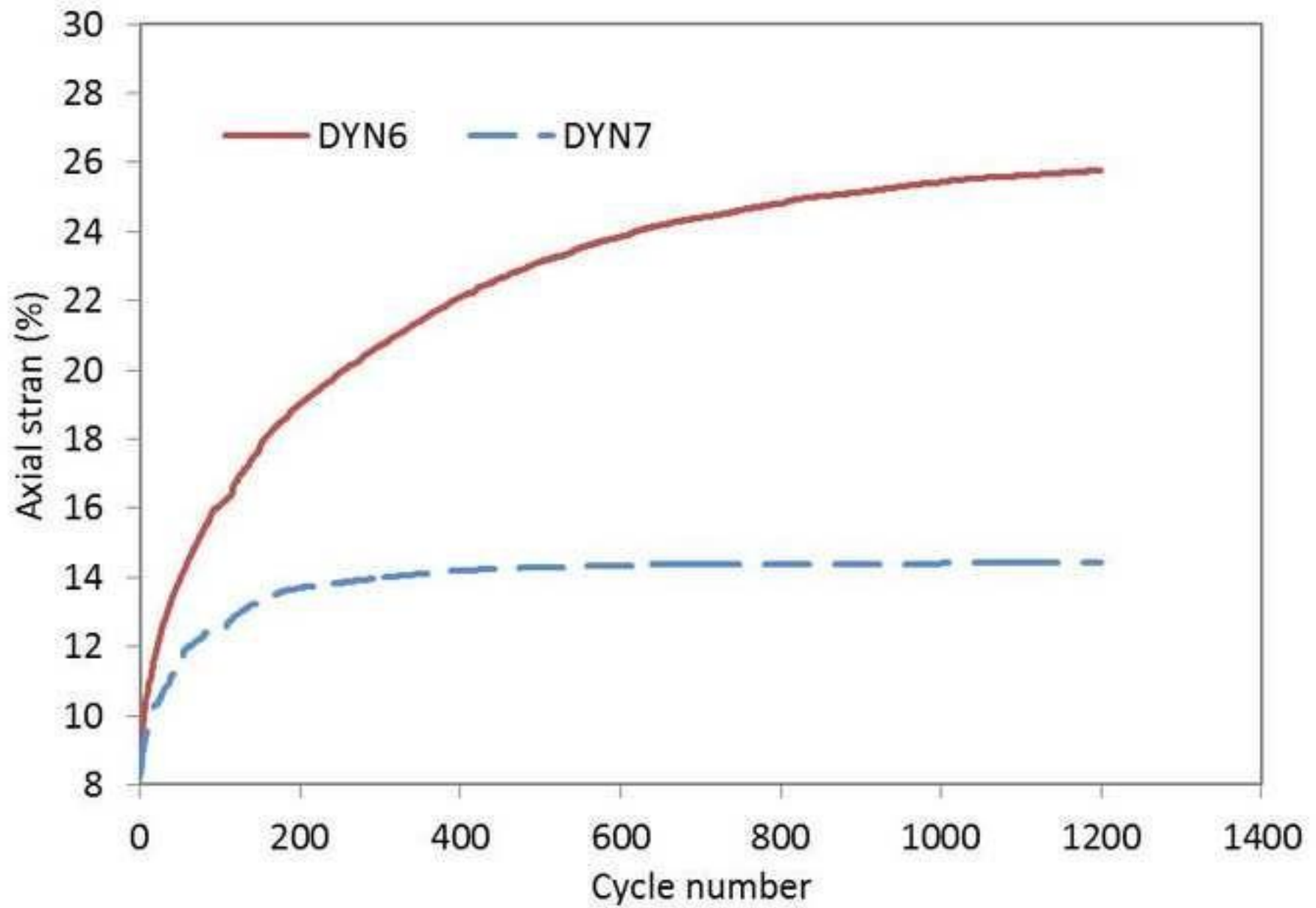


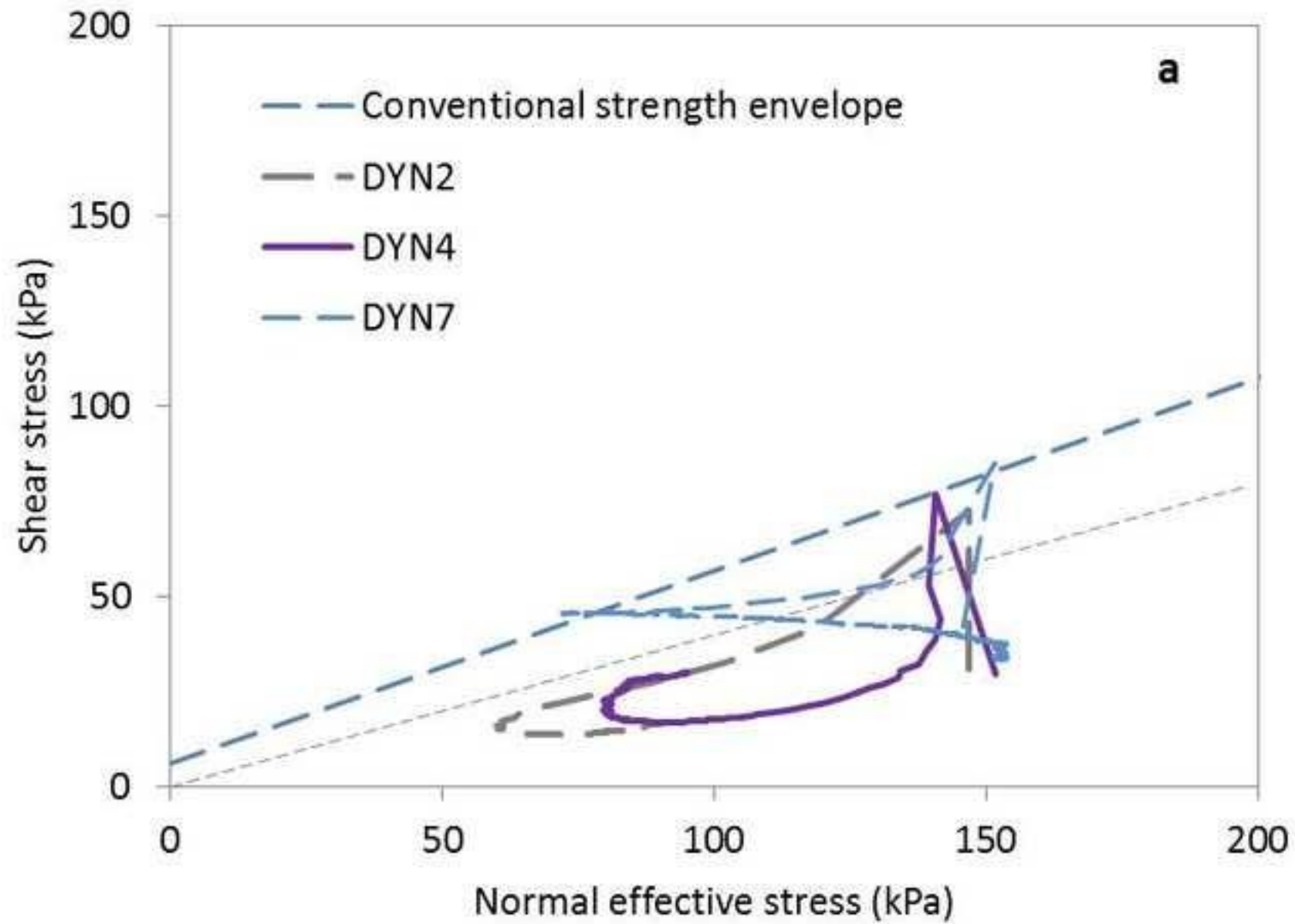
a

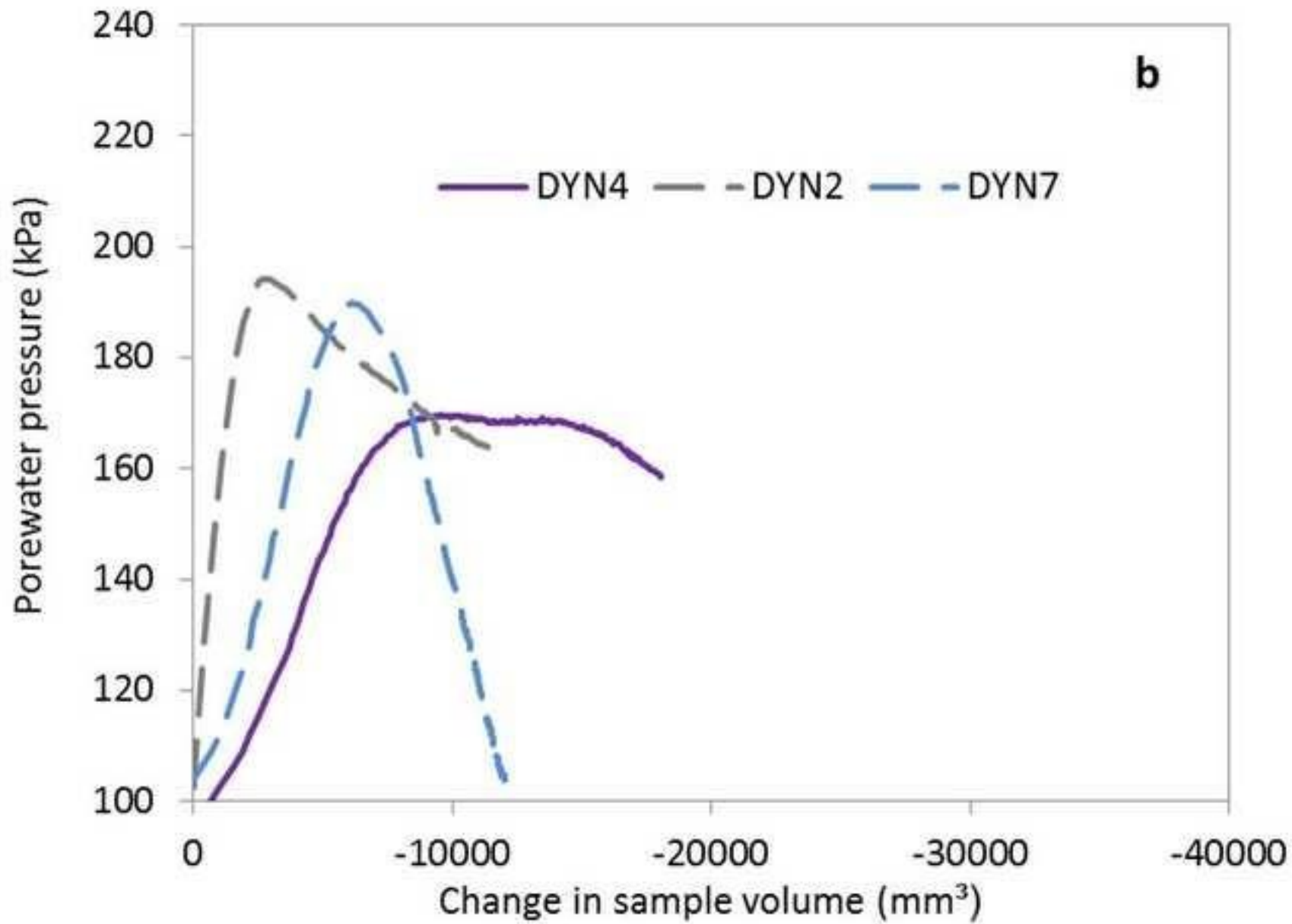


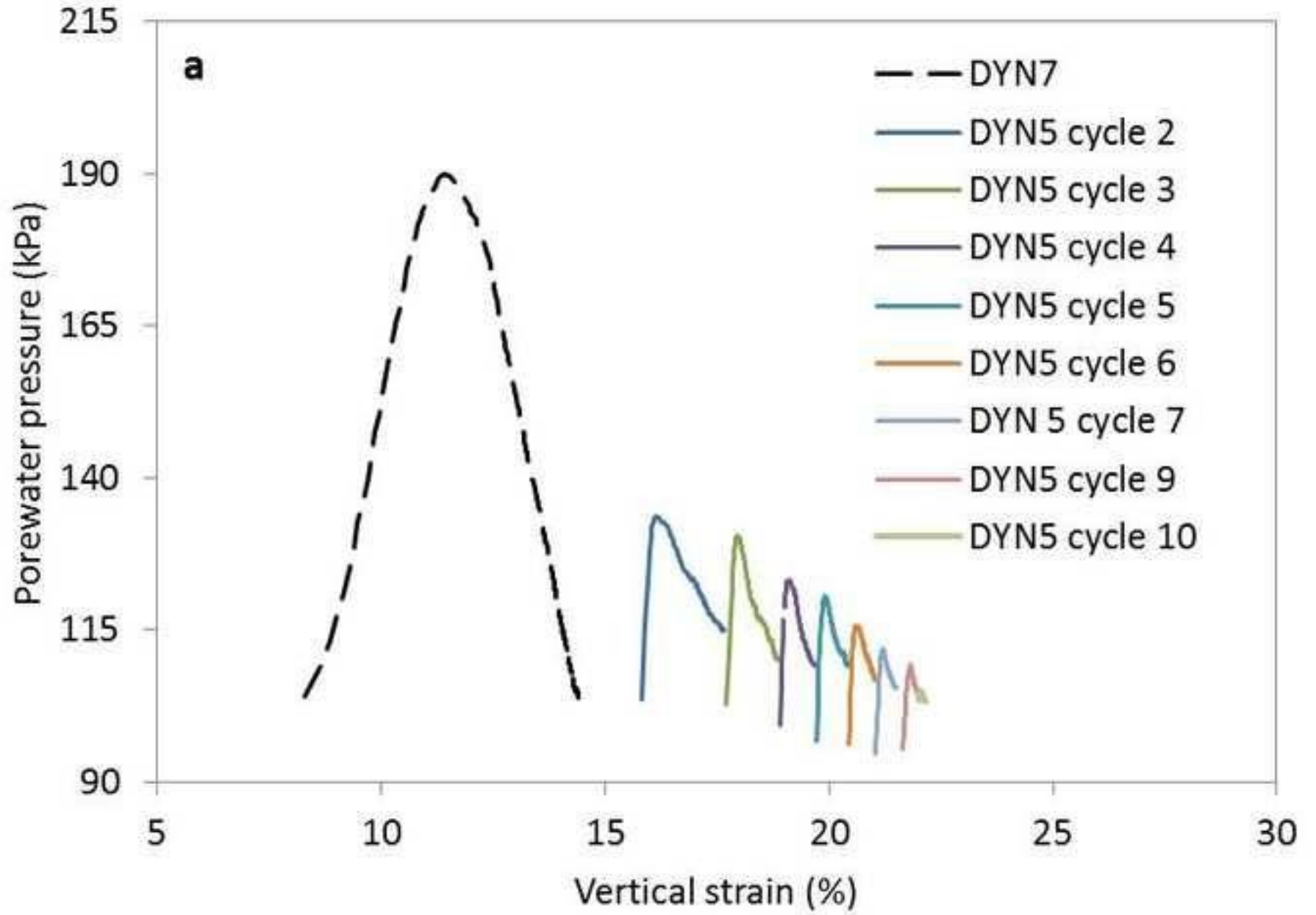


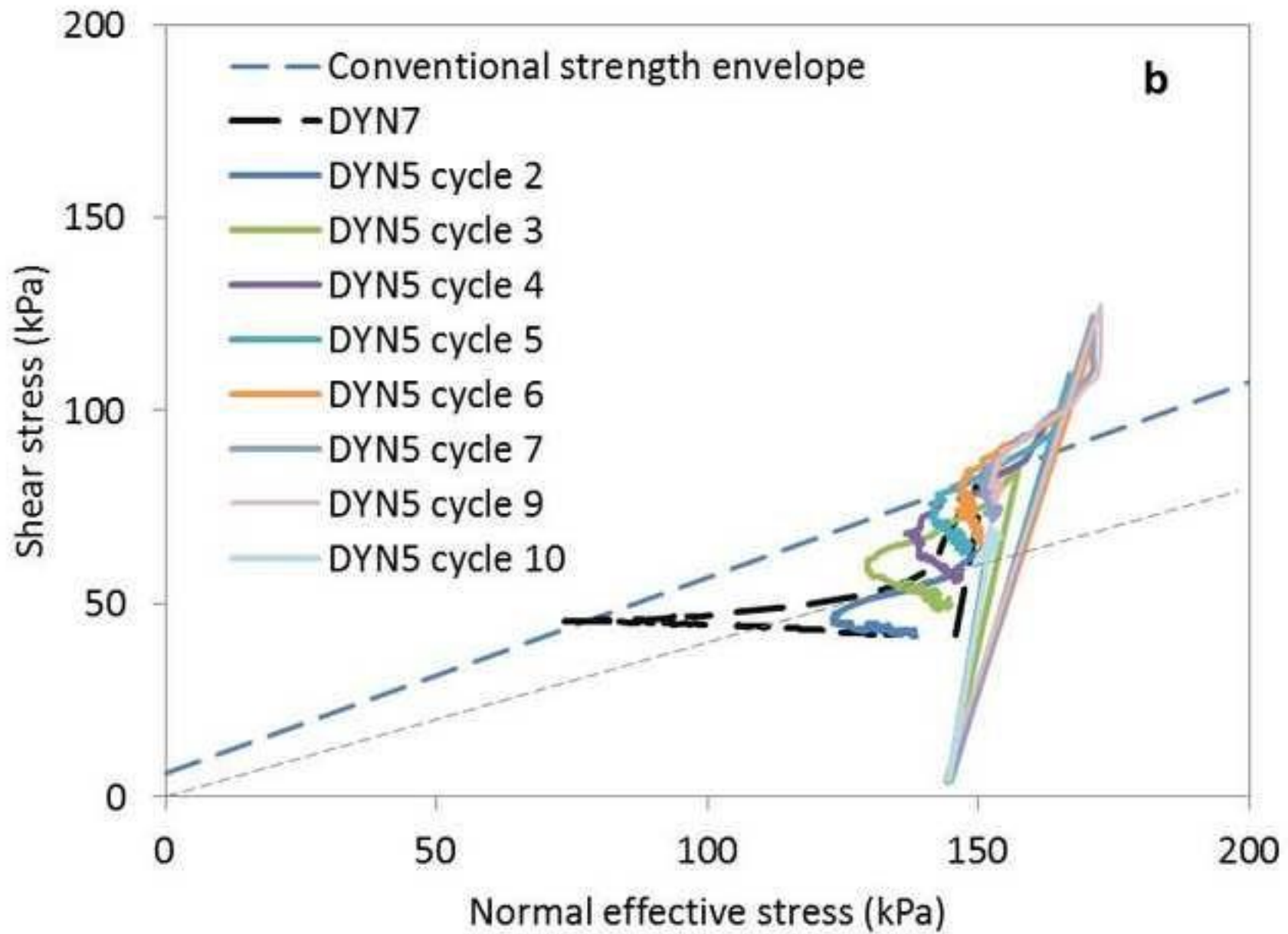












Physical property	Maffeys Road
Mc (%)	9.1
Liquid limit (%)	25
Plastic limit (%)	16
Plasticity index	9
Bulk density (mg/ m ³)	1.66 – 1.76
Dry density (Mg / m ³)	1.53 – 1.61
Initial void ratio	0.64 - 0.71

Sample Reference	Test type	Initial confining pressure (kPa)	Initial shear rate to 0.5 mm (mm/min)	Dynamic confining pressure (kPa)	Dynamic horizontal shear		Number of cycles (cycles x secs)
					Displacement +/- (mm)	Frequency (Hz)	
RS1	ring shear	154	0.0178	-	-	-	-
SB1	drained shear	148	0.01	-	-	-	-
SB2	undrained shear	148	0.01	-	-	-	-
DYN1	dynamic shear	150	0.01	150	0.5	1	60 (1 x 60)
DYN2	dynamic shear	150	0.01	150	0.5	2	120 (1 x 120)
DYN3	dynamic shear	150	0.01	150	0.5	3	180 (1 x 180)
DYN4	dynamic shear	150	0.01	150	0.5	4	240 (1 x 240)
DYN5	dynamic shear	150	0.01	150	0.5	2	600 (10 x 60)
DYN6	dynamic shear	150	0.01	150	0.5	2	600 (1 x 600)
DYN7*	dynamic shear	150	0.01	150	0.5	2	600 (1 x 600)

*remoulded sample